

Numerical Study on the Motion of Microscopic Oil Droplets in High Intensity Isotropic Turbulence

Murray R. Snyder^{a)}

*Department of Mechanical Engineering, The United States Naval Academy,
Annapolis, MD 21402-5042*

Omar M. Knio^{b)} and Joseph Katz^{c)}

*Department of Mechanical Engineering, The Johns Hopkins University,
Baltimore, MD 21218-2686*

Olivier P. Le Maître^{d)}

*Laboratoire d'Informatique pour la Mécanique et les Sciences de l'Ingénieur,
Centre National de la Recherche Scientifique (UPR3251), BP 133, F-91 403
Orsay, France*

Submitted to:

Physics of Fluids

Key Words: Turbulence, Droplets, Rise Velocity, Motion Coefficients

^{a)} Author to whom correspondence should be addressed. Email: msnyder@usna.edu

^{b)} Email: knio@jhu.edu

^{c)} Email: katz@jhu.edu

^{d)} Email: olm@limsi.fr

Suggested Running Head: Rise of oil droplets in isotropic turbulence

Mailing Address: Murray R. Snyder
Department of Mechanical Engineering
The United States Naval Academy
121 Blake Road, MS 11C
Annapolis, MD 21402-5042
Phone: (410) 533-8046; Fax: (410) 293-3041
Email: msnyder@usna.edu

ABSTRACT

The rise of small oil droplets in water under isotropic turbulence conditions is analyzed computationally. The effort focuses on the puzzling behavior observed by P. D. Friedman and J. Katz [Phys. Fluids **14**, 3059 (2002)], namely that the rise velocity of droplets smaller than $800\ \mu\text{m}$ in diameter is enhanced by turbulence whereas the rise of larger droplets is suppressed. Specifically, the study explores whether these effects can be captured or explained using a simplified one-way coupling model that combines DNS of the turbulent flow field with Lagrangian tracking of the droplets using a dynamical equation that accounts for buoyancy, virtual mass, pressure, drag, lift and history forces. The computational method used is adapted from the model of M. R. Snyder *et al.* [Phys. Fluids **19**, 065108 (2007)], which showed excellent correlation between computational results and extensive experimental data for microbubbles in isotropic turbulence. The computed results indicate that, using the quasi-steady, empirically-determined drag and lift coefficients, one is unable to reproduce the experimentally-observed droplet rise velocities. Numerical experiments on the effect of lift and history forces also indicates that, within a broad range of uncertainty, these forces do not account for the discrepancy between measured and computed trends. Guided by correlations obtained for the settling of heavy particles under high turbulence intensities, suppression of the drag and virtual mass coefficients for droplet diameters near ten times the Kolmogorov lengthscale was consequently postulated. Computed results indicate that, using this postulate, the simplified model is able to recover the observed enhancement of the mean rise of small droplets. These experiences underscore the difficulties in modeling the motion of small particles under high turbulence intensities, especially when the particle size is close to the turbulence microscale.

I Introduction

This paper is the second part of an effort concerning behavior of small particles (bubbles, droplets or solid particles) in isotropic turbulence. It is motivated by the puzzling behavior observed by Friedman and Katz,¹ namely that weakly-buoyant oil droplets in surfactant contaminated “tap” water rise faster in turbulence than in quiescent flow. This observed droplet behavior is not consistent with the generally accepted behavior of bubbles, where rise is suppressed by turbulence,^{2;3;4} nor with the generally accepted behavior of heavy particles, where settling is enhanced by turbulence.^{5;6;7}

In our prior work, Snyder *et al.*,⁸ the behavior of small bubbles in isotropic turbulence was studied using a simplified, one-way coupling model that combines direct numerical simulation of the flow field with a Lagrangian bubble equation of motion that accounts for buoyancy, added mass, pressure, drag, and lift forces. The results of these computations were shown to correspond well with available experimental data and prior computational studies on the behavior of bubbles in turbulence.

This paper investigates the question of whether such a simplified modeling approach can capture, and if so, explain the unexpected behavior observed by Friedman and Katz. Since slightly buoyant droplet force parametrization coefficients were not available, “numerical experiments” are performed to evaluate the impact of individual coefficients and combinations of coefficients that would explain the observed behavior.

A Overview of Experimental Results of Friedman and Katz

Friedman and Katz investigated the behavior of slightly buoyant oil droplets in surfactant contaminated water experiencing isotropic turbulence. They determined the rise rate of oil droplets in quiescent flow and under seven different isotropic turbulent fields (anisotropy in three perpendicular directions was observed to be less than 1% and 17%, respectively, for Friedman and Katz’s large test facility and small test facility). Observed dissipation rates were in the range $0.00055 \text{ m}^2/\text{sec}^3 \leq \tilde{\epsilon} \leq 0.11 \text{ m}^2/\text{sec}^3$ and Kolmogorov microscales were in the range $60 \text{ }\mu\text{m} \leq \tilde{\eta} \leq 180 \text{ }\mu\text{m}$. (Tildes are used to represent dimensional quantities.) Figure 1 shows the experimentally-observed quiescent rise velocities obtained by Friedman and Katz, which are very close to calculated rise rates using a solid sphere drag coefficient. Figure 2 depicts the observed turbulent rise velocity normalized by quiescent rise velocity for Friedman and Katz’s large facility L3 with $\tilde{\epsilon}$ of $0.0086 \text{ m}^2/\text{sec}^3$ and $\tilde{\eta}$ of $88 \text{ }\mu\text{m}$.

The droplet behavior exhibited in Figure 2 can also be shown in terms of observed mean rise velocities plotted against droplet size. Figure 3 shows the Friedman and Katz large facility L3 experimental results along with the droplet quiescent rise rate calculated using the drag relationship determined by Feng and Michaelides⁹ for finite droplet Reynolds numbers ($0.5 \leq Re_d \leq 1000$) with a viscosity ratio $\lambda = 6.4$, where $\lambda \equiv \tilde{\mu}_i/\tilde{\mu}_e$ is the ratio between the viscosity of the droplet fluid and that of the water. In Figure 1, Friedman and Katz provide

the calculated rise rate for a viscosity ratio of 6.4, though their calculation was based on a Stokes flow ($Re_d \ll 1$) model. (A detailed discussion of the Feng and Michaelides drag relationship will be provided later.) The viscosity ratio of 6.4 corresponds to the research grade fuel oil and fresh water used in the experiments.

As mentioned previously, there is wide agreement in the literature that the rise of microbubbles is suppressed by turbulence and the settling of heavy particles is enhanced by turbulence. Consequently, the behavior exhibited for slightly buoyant oil droplets as shown Figure 2 is particularly unexpected and obviously not intuitive. Note that slightly buoyant oil droplets with diameter less than approximately $800 \mu\text{m}$ exhibit average turbulence rise rates higher than corresponding quiescent velocities. Conversely, droplets with diameter greater than approximately $800 \mu\text{m}$ exhibit the reverse behavior, *i.e.* droplet rise rates were suppressed in turbulence as compared to those in quiescent conditions. Friedman and Katz theorized that upwards trajectory biasing, or the sweeping of droplets to the *up-flow* side of turbulent eddies, “is the only known mechanism capable of this enhancement [of droplet rise velocity]...under the present range of parameters.” It is well established that downwards trajectory biasing, or sweeping to the *down-flow* side of turbulent eddies, is responsible for the enhancement of heavy particle settling and retardation of microbubbles rise in turbulence.^{5;6;7;2}

Note the puzzling behavior observed by Friedman and Katz does not appear to be a “unique” phenomenon. Specifically, similarities exist between the velocity trends measured by Friedman and Katz and the experimental observations of Nocentini and Magelli,¹⁰ who analyzed the settling of glass and plastic spheres in a continuously stirred water tank. Figure 4 reproduces some of the data reported by Nocentini and Magelli, which reveals a sudden change in the particle settling velocity for diameters around 10 times the Kolmogorov microscale. The similarity between the experimental trends of Friedman and Katz and of Nocentini and Magelli suggests that the corresponding observations are not isolated anomalous phenomena. Our attention, however, is exclusively focused on the behavior of the oil droplets.

B Outline

A sketch of the computational approach adopted in the present investigation is provided in Sec. II. Description of the flow solver is omitted, but a brief description of the Lagrangian method for tracking droplet behavior is provided.

As it is evident that success of the Lagrangian tracking approach depends on the use of realistic motion coefficients, a discussion is provided in Sec. III of their selection. In particular, the discussion covers selection of “baseline” values for the drag, lift and virtual mass coefficients. Unfortunately, computations performed using these baseline values yield results that are inconsistent with the experimental observations of Friedman and Katz, with large discrepancies between predicted and measured mean rise velocities.

Consequently, systematic numerical experiments have been performed in order to determine the origin of the discrepancy between predictions and experiments, particularly to investigate the effects of parametric uncertainties in correlations used to represent various forces acting on the droplets.

In Sec. IV, uncertainty in the lift coefficient is considered, and numerous experiments are performed in order to assess its effect on the predictions. Although a wide range of parameters was considered, the experimental behavior could not be reproduced. A similar analysis is performed in Sec. V of the effect of the history force coefficient. The analysis shows that, in the regime considered, variation of the history coefficient within a large range has weak impact on the predictions.

In Sec. VI, the impact of the drag coefficient is analyzed. We start with a review of relevant experimental data which indicates that at high turbulence intensities, the mean drag coefficient experienced by small particles can differ significantly from the quasi-steady local value. This review is then used to suggest a modified drag behavior and numerical experiments are performed to investigate the impact of such modification. Mean rise velocities obtained with the modified drag coefficient are found in closer agreement with experimental predictions than those obtained with baseline drag coefficient, though substantial discrepancies can still be observed.

In Sec. VII, the impact of the virtual mass coefficient is analyzed. In particular, by postulating a suppression in the virtual coefficients for droplets smaller than $800\ \mu\text{m}$ diameter, with the modified drag behavior, mean rise predictions are obtained that are in reasonable agreement with experimental observations.

Though not providing conclusive evidence concerting the validity of fundamental correlations, the present experiences point to substantial uncertainties in modeling the motion of small particles in turbulent flow. This and other conclusions of this study are discussed in Sec. VIII.

II Numerical Approach

As mentioned previously, we rely on a simplified, one-way coupling model that combines DNS of the flow field with Lagrangian tracking of the droplets. The model assumes very small void fractions and, consistent with our prior work⁸ and that of others,^{11;12;13;14} ignores the impact of droplets on the turbulent flow as well as droplet interactions. We rely on one-way coupling because this approach enables us to efficiently perform a large number of parallel realizations using the same turbulence field, which is essential for the present analysis. In addition, our prior work⁸ showed that the resulting computations yielded excellent correlations with available computations and experimental data for microbubbles in turbulence. The DNS is based on a pseudospectral flow solver that is used to simulate the isotropic turbulent flow. Details can be found in Snyder *et al.*⁸ and Snyder.¹⁵ The Lagrangian tracking of the droplets is based on a dynamical equation of motion that accounts for drag, lift, added mass and history forces. A brief outline of the corresponding dynamical model is provided

below.

A Lagrangian Equation of Motion

Following Maxey and Riley¹⁶ and others,^{17;18;19;13;15} the non-dimensional equations of motion of small droplets can be expressed as:

$$\left\{ \begin{array}{l} \frac{d\mathbf{X}_d}{dt} = \mathbf{V}_d(t), \\ \frac{d\mathbf{V}_d}{dt} = -2\Delta\rho^* \mathbf{g} + \left(\frac{\tilde{\rho} + C_{VM}\tilde{\rho}}{\tilde{\rho}_d + C_{VM}\tilde{\rho}} \right) \frac{D\mathbf{u}}{Dt} + \frac{3\rho^*}{4a} \left[C_D |\mathbf{u}_r| \mathbf{u}_r + C_L \frac{|\mathbf{u}_r|}{|\boldsymbol{\omega}|} \mathbf{u}_r \wedge \boldsymbol{\omega} \right] \\ \quad + C_H \frac{9}{\sqrt{\pi Re}} \frac{\rho^*}{a} \int_0^t \frac{d\mathbf{u}_r/d\tau}{\sqrt{t-\tau}} d\tau \end{array} \right. \quad (1)$$

where $\mathbf{X}_d(t)$, $\mathbf{V}_d(t)$, $\tilde{\rho}_d$, a , C_D , C_L , C_{VM} , C_H respectively denote the droplet position, velocity, density, radius ($d_d/2$), drag coefficient, lift coefficient, virtual mass coefficient, and history force coefficient, $\tilde{\rho}$ is the fluid density,

$$\rho^* \equiv \frac{1}{2} \left(\frac{\tilde{\rho}}{\tilde{\rho}_d + C_{VM}\tilde{\rho}} \right) \quad (2)$$

is the reduced density,

$$\Delta\rho^* \equiv \frac{1}{2} \left(\frac{\tilde{\rho} - \tilde{\rho}_d}{\tilde{\rho}_d + C_{VM}\tilde{\rho}} \right) \quad (3)$$

is the reduced density difference, ω is the normalized local vorticity at the droplet position, $\mathbf{u}_r \equiv \mathbf{u} - \mathbf{V}_d$ is the normalized relative velocity (field velocity less droplet velocity), and $Re \equiv U^c L^c / \bar{\nu}$ is the flow Reynolds number. Re , set to 1000, and the dimensionless dissipation rate, $\varepsilon = 4.0 \times 10^{-3}$, fix the normalized Kolmogorov microscale at $\eta \equiv (\varepsilon Re^3)^{-1/4} \approx 0.022$ in $(2\pi)^3$ spectral space. This provides sufficient resolution to match the flow characteristics in the experiments of Friedman and Katz. The field velocity \mathbf{u} is determined using a linear interpolation of the velocity field at the droplet position, using the velocities at the surrounding grid points. Variables are normalized with respect to the appropriate combination of reference length, velocity and time scales, respectively L^c , U^c , and $t^c \equiv L^c/U^c$.

Integration of the droplet equations of motion is performed using the implicit-explicit approach of Cerutti *et al.*,¹³ described in detail in Snyder *et al.*⁸ This method uses an implicit, Crank-Nicolson treatment of the linear part of the drag term, and an explicit treatment of the remaining terms. The advantage of this method is that it overcomes the inherent stiffness of the equation of motion when droplet Reynolds numbers are small.

B Simulation of Large Faculty L3 Turbulent Field

Turbulence intensity of the simulation was approximately matched with Friedman and Katz's large facility L3 Kolmogorov microscale of 88 μm according to:

$$\tilde{\eta} = \eta L^c$$

where $\tilde{\eta}$ is the dimensional Kolmogorov microscale, η is the normalized or dimensionless Kolmogorov microscale and L^c is the characteristic length scale. (Friedman and Katz reported L3 dissipation as $\tilde{\epsilon} = 0.0086 \text{ m}^2/\text{sec}^3$ while the simulation has $\tilde{\epsilon} = 0.016 \text{ m}^2/\text{sec}^3$. The difference arises from Friedman and Katz calculating dissipation using kinematic viscosity $\tilde{\nu} = 0.8 \times 10^{-6} \text{ m}^2/\text{sec}$ (value for water at 30°C) while the simulation used $\tilde{\nu} = 1.0 \times 10^{-6} \text{ m}^2/\text{sec}$ (value for water at 20°C). The viscosity of water at 20°C was used since this is the approximate temperature observed in the L3 facility during more recent testing.)

As discussed in Snyder *et al.*,⁸ the reference length scale is selected so that the normalized domain length equals 2π . In other words, $L^c = \tilde{L}/2\pi$, where \tilde{L} is the physical domain length. The characteristic length and velocity are given in Table 1, together with additional properties of the turbulent velocity field.

Oil droplets with radii of 100, 200, 250, 300, 350, 400, 450, 500, 600 and 700 μm were then simulated. Consistent with the normalization convention, the normalized droplet radius appearing in (1) is obtained from $a = \tilde{a}2\pi/\tilde{L}$. Thus, for a 700 μm radius, $a=0.176$.

III Baseline Coefficients and Baseline Predictions

In this section, we compare initial predictions with the experimental data of Friedman and Katz. These predictions are based on the use of “baseline” coefficients in the force correlations appearing in the droplet equation of motion (1). These preliminary coefficients, and the rationale for their selection, are detailed below.

A Coefficient of Drag

There are no known experimental correlations for drag of slightly buoyant oil droplets in water. The drag correlation of Feng and Michaelides⁹ was selected since it accounts for the interaction between the viscous oil droplets and the less viscous carrier fluid (water); we consequently match the viscosity ratio in the experiments of Friedman and Katz.

The Feng and Michaelides drag correlation follows:

$$\left\{ \begin{array}{l} C_D = \frac{8}{Re_d} \frac{3\lambda + 2}{\lambda + 1} \left(1 + 0.05 \frac{3\lambda + 2}{\lambda + 1} Re_d \right) - 0.01 \frac{3\lambda + 2}{\lambda + 1} Re_d \ln(Re_d), \\ 0 \leq Re_d \leq 5, \quad 0 \leq \lambda \leq \infty \\ C_D = \frac{4}{\lambda + 2} C_D(Re_d, 2) + \frac{\lambda - 2}{\lambda + 2} C_D(Re_d, \infty), \\ 5 < Re_d \leq 1000, \quad 2 \leq \lambda \leq \infty \end{array} \right. \quad (4)$$

where $\lambda = \tilde{\mu}_i/\tilde{\mu}_e$ is the ratio of interior (droplet) and exterior (carrier fluid) viscosities, and $C_D(Re_d, 2)$ and $C_D(Re_d, \infty)$ are given by:

$$\left\{ \begin{array}{l} C_D(Re_d, 2) = 17.0 Re_d^{-2/3} \\ C_D(Re_d, \infty) = \frac{24}{Re_d} \left(1 + \frac{1}{6} Re_d^{2/3} \right) \end{array} \right. \quad (5)$$

The Feng and Michaelides drag correlation assumes that the viscous droplet remains spherical or nearly spherical, even at high Re_d . (At sufficiently high Re_d , and hence sufficiently large relative velocities, the droplets have the tendency to become oblate, or flatten, which can significantly alter the drag on the droplet.) Winnikow and Chao²⁰ performed experiments on the rise and fall of drops in liquids and determined that drops remain spherical if the dimensionless Bond number, Bo , remains smaller than 0.2, *i.e.*

$$Bo \equiv \frac{\mathbf{G} \tilde{d}^2 |\tilde{\rho}_d - \tilde{\rho}_f|}{\tilde{\sigma}} \leq 0.2 \quad (6)$$

where \mathbf{G} is the acceleration of gravity, \tilde{d} is droplet diameter, $|\tilde{\rho}_d - \tilde{\rho}_f|$ is the magnitude of the density difference between the droplet and the surrounding carrier fluid, and $\tilde{\sigma}$ is the surface or interfacial tension of the droplet.

Further, following the results of Harper²¹ and the analyses of Leal²² and of Feng and Michaelides, it can be shown that for $Bo < 0.4$, the error in the drag correlation of Feng and Michaelides due to a non-spherical shape is less than 5 percent. Snyder¹⁵ showed that for a 700 μm radius droplet $Bo \cong 0.22$, allowing one to conclude that the Feng and Michaelides drag correlation can be used for modeling droplet behavior in the considered range of 100-700 μm droplet radii.

Additionally, the Feng and Michaelides drag correlation yields very good correlation with the Friedman and Katz experimental oil droplet rise data under quiescent conditions. This is depicted in Figure 5, which compares the quiescent droplet rise rate obtained using the Feng and Michaelides drag correlation with the quiescent rise experimental data.

One should note that the C_D determined using the Feng and Michaelides correlation does not differ by more than approximately 50% from that calculated

using the widely used drag correlations for solid spheres (see, for example, Crowe *et al.*¹⁹), namely

$$C_D = \frac{24}{Re} (1 + 0.15Re^{0.687}), \quad Re \lesssim 800 \quad (7)$$

or

$$C_D = \frac{24}{Re} \left(1 + \frac{Re^{2/3}}{6} \right), \quad Re < 1000 \quad (8)$$

Figure 6 shows a comparison of the Feng and Michaelides correlation (4) for droplets with the standard drag correlation (7) for spheres in the range $1 \leq Re \leq 800$. Inspection reveals differences, increasing with increasing Re_d , between the two drag correlation curves of up to approximately 50% at $Re_d = 800$. However, as will be shown later, use of the standard sphere drag correlation instead of the Feng and Michaelides drag correlation does not significantly alter simulation results.

B Coefficient of Lift

There are no known experimental correlations for lift of slightly buoyant oil droplets in water. The lift correlation of Kurose and Komori²³ for a sphere in linear shear flow was selected as baseline correlation.

Kurose and Komori determined that C_L varied as function of Re , dimensionless shear α^* and rotational angular speed Ω^* . Their correlation is related to the Magnus effect,²⁴ where a spinning object creates regions of enhanced (and reduced) local fluid velocity due to a no slip boundary condition on the surface of the object. Specifically, Kurose and Komori proposed the following lift correlation for $Re_p = 1, 5, 10, 50, 100, 200, 300, 400$ and 500:

$$C_L(Re_p, \alpha^*, \Omega^*) = K_0 \alpha^{*0.9} + K_1 \alpha^{*1.1} + (K_2 + K_3 \alpha^* + K_4 \alpha^{*2.0} + K_5 \alpha^{*9.5}) \Omega^* \quad (9)$$

where

$$\alpha^* = \frac{\tilde{a}}{U_c} \frac{\partial U}{\partial y} \quad (10)$$

is the dimensionless shear, U_c is the centerline velocity and $U(y)$ is the shear velocity, and

$$\Omega^* = \frac{\tilde{a}}{U_c} \Omega \quad (11)$$

is the dimensionless rotational angular speed, Ω the angular speed of the sphere, and K_0, K_1, K_2, K_3, K_4 and K_5 are constants, which are dependent upon Re_p . K_0 and K_4 are primarily negative while K_1, K_2, K_3 and K_5 are primarily positive, which allows for both positive and negative C_L as Re_p and α^* vary.

As shown in Figure 7, the correlation of Kurose and Komori predicts that C_L changes from positive to negative for both a stationary and rotating sphere in the range $10^1 \leq Re_p \leq 10^2$, where Re_p is the Reynolds number of the sphere. This is also the range of droplet Reynolds numbers where Friedman and Katz observed the transition from turbulence enhanced rise to turbulence retarded rise. This feature motivates its selection as baseline correlation.

Note that the dimensionless shear can also be defined as $\alpha^* = a|\boldsymbol{\omega}|/|\mathbf{u}_r|$, where $\boldsymbol{\omega}$ is normalized vorticity and \mathbf{u}_r is normalized relative velocity. Consequently, and since α^* , Re_d , $\boldsymbol{\omega}$ and \mathbf{u}_r are calculated for each droplet at each time step in the simulation, the first two terms in (9) can readily be calculated. The rotational speed of the droplets cannot be determined from the present model. However, the first two terms in (9) should dominate except at very high droplet rotational speeds. Assuming that droplet rotation is not significant, the baseline C_L was then modeled as

$$C_L(Re_p, \alpha^*) = K_0 \alpha^{*0.9} + K_1 \alpha^{*1.1} \quad (12)$$

C Coefficient of Virtual Mass

$C_{VM} = 1/2$, the theoretical value for an ideal inviscid flow, was selected for baseline behavior, though there are no known experimental results that support using this correlation for slightly buoyant oil droplets in turbulent flows. Most prior numerical studies of microbubble or particle behavior^{2;3;6;13;25;26;27} have generally either assumed the inviscid value ($C_{VM} = 1/2$) or have ignored the virtual mass force (*e.g.* $C_{VM} = 0$). In particular, in our own prior work,⁸ a virtual mass coefficient of $1/2$ was used for the simulation of microbubble motion and dispersion in isotropic turbulence. Since our predictions showed very good agreement with experimental microbubble measurements, a virtual mass coefficient of $1/2$ is used as baseline value for droplets.

D Coefficient of History Force

$C_H = 0$ was selected for baseline behavior. Most prior numerical studies of heavy particles and microbubbles^{2;3;6;13;25;26} have neglected the history force

as it has been shown to be generally very small compared to the other forces in the equation of motion. For instance, Sridhar and Katz¹⁸ showed that for microbubbles entrained in a vortex the history force is only approximately 16% of the lift force and approximately 6% of the drag force.

E Baseline Predictions

A simulation was performed using the baseline coefficients above, and predictions of mean droplet rise velocities are shown in Figure 8. Also plotted for comparison are rise rates for droplets under quiescent conditions and the experimental results of Friedman and Katz for droplets in turbulence. The computed trends are similar to those of microbubbles in isotropic turbulence, namely that turbulence suppresses the rise velocity for all droplet radii.

Figure 8 indicates that the baseline simulation results diverge significantly from the experimental results of Friedman and Katz. Specifically, baseline predictions are significantly lower than measured for droplets $\leq 800 \mu\text{m}$ in diameter, with errors as high as $\approx 75\%$ for the smallest diameters studied. Conversely, for droplet diameters larger than $800 \mu\text{m}$, the predicted rise velocities exceed the experimental data by up to $\approx 50\%$.

It is possible that a portion of the large discrepancies observed arise from the simplified representation of the underlying flow; though, in our prior work,⁸ the same numerical simulation correctly predicted the behavior of microbubbles in isotropic turbulence. Consequently, and since the baseline coefficients showed such large discrepancies compared with experimental mean rise behavior, a systematic study of the impact of varying the motion coefficients and/or force correlation was then undertaken, as further discussed below.

IV Numerical Experimentation in the Variation of the Lift Coefficient

In this section, different lift coefficients are considered in order to determine their impact on droplet rise in turbulence. Simulations were performed using the Kurose and Komori variable lift C_L with the Feng and Michaelides C_D , twice this same C_L (again with the Feng and Michaelides C_D), twice the experimentally-determined air bubble C_L of Sridhar and Katz,¹⁷

$$C_L = 0.59 \left(\frac{a|\boldsymbol{\omega}|}{|\mathbf{u}_r|} \right)^{1/4},$$

with the Feng and Michaelides C_D , $C_L = 0$ with the air bubble C_D of Cerutti *et al.*,¹³ the air bubble C_L and C_D , and the Kurose and Komori C_L with the air bubble C_D . Results are shown in Figure 9, inspection of which reveals only small differences between the various combinations of C_L and C_D . None of the C_L and C_D combinations correctly capture the experimental behavior observed by Friedman and Katz. Specifically, there is no enhancement of rise for droplets

smaller than $400 \mu\text{m}$ radii and the calculated suppression of rise for droplets larger than $400 \mu\text{m}$ radii is significantly smaller than in the experimental observations.

Based upon simulation results, one can conclude that the large variations in the lift force considered in the numerical experiments above do not explain the observed rise behavior of Friedman and Katz. Further, and contrary to the mechanism postulated by Friedman and Katz, the present experiments do not provide any evidence that the lift force may be responsible for enhancement of droplet rise velocity.

Statistics of the lift force for the baseline simulation (Feng and Michaelides C_D and Kurose and Komori C_L) are provided in Table 2. Analysis of this data reveals that the magnitude of the lift force is very small (*e.g.* $\lesssim 5\%$) compared to the magnitude of the mean drag force. Figure 10 shows probability density functions (pdfs) of the lift force in the vertical direction, which are increasingly skewed towards positive values as droplet radius increases. These pdfs show that the lift force does not enhance vertical rise rate for bubbles $\lesssim 300 \mu\text{m}$ radius. For larger droplets the lift force enhances vertical rise, though the impact is very small compared to the impact of the drag force. Similarly skewed pdfs were observed in our prior work for microbubbles in isotropic turbulence.⁸

V Numerical Experiments of the Effect of the History Force Coefficient

In this section, the impact of variation in the history force is investigated. A brief background of the history force is first provided.

A Background

The original description of the interaction of a particle with its own wake was described by Basset²⁸ for flow over a sphere at low Re . Under these conditions, Basset defines the history force as

$$F_H = 6\tilde{a}^2 \sqrt{\pi\tilde{\rho}_c\tilde{\mu}_c} \int_0^{\tilde{t}} \frac{d(U_R)/d\tilde{\tau}}{\sqrt{\tilde{t}-\tilde{\tau}}} d\tilde{\tau} \quad (13)$$

where $d(U_R)/d\tilde{\tau}$ is the relative acceleration of the particle, $\tilde{\rho}_c$ is the carrier fluid density, and $\tilde{\mu}_c$ is the carrier fluid dynamic viscosity.

The Basset force is often described as a ‘‘history’’ force since it depends upon the acceleration felt by the bubble or droplet during past time.

Reeks and McKee²⁹ showed that equation (13) needs to be modified in order to account for a non-vanishing initial relative velocity. To this end, the history force is expressed as:

$$F_H = 6\tilde{a}^2 \sqrt{\pi\tilde{\rho}_c\tilde{\mu}_c} \left[\int_0^{\tilde{t}} \frac{d(U_R)/d\tilde{\tau}}{\sqrt{\tilde{t}-\tilde{\tau}}} d\tilde{\tau} + \frac{U_{Ro}}{\sqrt{\tilde{t}}} \right] \quad (14)$$

where U_{Ro} is the initial difference in relative velocity. However, Reeks and McKee noted that if the velocity decay is greater than $\tilde{t}^{-1/2}$ then the additional term would not occur.

The history force, neglecting the initial relative velocity difference, is also often written as a function of the history kernel $K(\tilde{t}, \tilde{\tau})$

$$F_H = \tilde{a}\tilde{\mu}_c \int_0^{\tilde{t}} K(\tilde{t}, \tilde{\tau}) \frac{d(U_R)}{d\tilde{\tau}} d\tilde{\tau} \quad (15)$$

where, for the original Basset expression

$$K(\tilde{t}, \tilde{\tau}) = 6 \left(\frac{\pi \tilde{a}^2}{\tilde{\nu}_c (\tilde{t} - \tilde{\tau})} \right)^{\frac{1}{2}} \quad (16)$$

with $\tilde{\nu}_c \equiv \tilde{\mu}_c / \tilde{\rho}_c$ the kinematic viscosity of the carrier fluid.

For a bubble, Yang and Leal,³⁰ provide a similar but alternate form of the history kernel

$$K(\tilde{t}, \tilde{\tau}) = \frac{1}{2} \pi \exp \left(\frac{36 \tilde{\nu}_c (\tilde{t} - \tilde{\tau})}{\tilde{a}^2} \right) \operatorname{erf} \left(\frac{36 \tilde{\nu}_c (\tilde{t} - \tilde{\tau})}{\tilde{a}^2} \right) \quad (17)$$

Lovalenti and Brady³¹ further showed that, for a droplet with kinematic viscosity differing from that of the surrounding fluid, a closed form of the history kernel $K(\tilde{t}, \tilde{\tau})$ as $Re_d \rightarrow 0$ is not obtainable.

For flows with finite Re , several studies have shown that the large-time decay of the history kernel is faster than $\tilde{t}^{-1/2}$, though the specific form of the kernel is not fixed. Mei *et al.*³² analyzed unsteady flow over a stationary sphere at finite Re_p ($0.1 \leq Re_p \leq 40$) and showed that the history kernel decays much faster than $\tilde{t}^{-1/2}$. They further theorized that the “unphysical” results found by Reeks and McKee,²⁹ where the history force also depends upon the initial relative velocity difference, are due to the history kernel actually decaying quicker than $\tilde{t}^{-1/2}$.

For bodies with Re of $O(1)$ in arbitrary motion in an uniform flow, Lovalenti and Brady³³ showed that the history kernel exhibits both algebraic and exponential decay in response to step changes in the speed of the body. Specifically, the kernel exhibits

1. a \tilde{t}^{-2} temporal decay for a body accelerating from rest,
2. a \tilde{t}^{-1} temporal decay for a body coming to an abrupt stop, and
3. a $e^{-\tilde{t}}$ temporal decay for a body between the extremes of accelerating from rest and coming to an abrupt stop.

For bodies of finite Re undergoing rectilinear motion, Lawrence and Mei³⁴ showed similar results with the kernel decaying algebraically, either \tilde{t}^{-1} or \tilde{t}^{-2} . They obtained \tilde{t}^{-1} when the body was brought to rest or when the body reverses motion. Under other conditions they obtained \tilde{t}^{-2} temporal decay.

Kim *et al.*³⁵ proposed a new model for history force over $2 < Re < 150$ for particles heavier than the fluid (particle to fluid density ratio of 5 to 200). The model was limited to studying the deceleration of a sphere injected into an initially stationary or oscillating fluid. Their history kernel has both $\tilde{t}^{-1/2}$ and \tilde{t}^{-2} temporal decay terms. As $Re \rightarrow 1$, their history kernel recovers the same form as that of Basset. When $Re \gg O(1)$, however, the \tilde{t}^{-2} term dominates.

Finally, Bagchi and Balachandar³⁶ have shown for flows with shear, strain, or rotation, $K(\tilde{t}, \tilde{\tau})$ must depend upon the velocity gradient in addition to the time variation.

B Parameterization of the History Force

Parameterization of the history kernel for numerical simulations of droplets in unsteady flows is quite challenging. The Basset $\tilde{t}^{-1/2}$ temporal decay is only valid for Stokes flow ($Re_d \rightarrow 0$). Also, the history force as modified by Reeks and McKee for homogeneous turbulent flows, would not be valid as their initial relative velocity term does not occur if the temporal decay is greater than $\tilde{t}^{-1/2}$. Finally, the appropriate history kernel or temporal decay for $Re_d > 1$ varies as a function of droplet motion, namely according to whether the droplet is accelerating, decelerating, coming to rest, or reversing direction.

Since there is no closed form of the history force that applies to all possible droplet behaviors, the classical Basset integral, with $\tilde{t}^{-1/2}$ temporal decay, was used with a finite time history to model the decay of the history force as greater than $\tilde{t}^{-1/2}$. Following Berezin and Zhidkov,³⁷ Chung³⁸ and Kim *et al.*,³⁵ the following quadrature is used in approximating the associated convolution integral:

$$\begin{aligned} \int_0^t \frac{\mathbf{u}_r}{\sqrt{t-\tau}} d\tau &= \int_0^{n\Delta t} \frac{\mathbf{u}_r}{\sqrt{t-\tau}} d\tau \\ &\approx \frac{\Delta t}{6} \sum_{i=1}^{n-1} \left[\frac{\mathbf{u}_{ri-1}}{\sqrt{n\Delta t - (i-1)\Delta t}} + \frac{2(\mathbf{u}_{ri-1} + \mathbf{u}_{ri})}{\sqrt{n\Delta t - (i-0.5)\Delta t}} + \frac{\mathbf{u}_{ri}}{\sqrt{n\Delta t - i\Delta t}} \right] \\ &\quad + \frac{0.9\Delta t}{6} \left[\frac{\mathbf{u}_{rn-1}}{\sqrt{\Delta t}} + \frac{2(\mathbf{u}_{rn-1} + \mathbf{u}_{rn})}{\sqrt{0.55\Delta t}} + \frac{\mathbf{u}_{rn}}{\sqrt{0.1\Delta t}} \right] \\ &\quad + \frac{0.1\Delta t}{2} \left[\frac{8\sqrt{2}}{3} \frac{\mathbf{u}_{rn}}{\sqrt{0.05\Delta t}} - \frac{4}{3} \frac{\mathbf{u}_{rn}}{\sqrt{0.1\Delta t}} \right] \end{aligned} \tag{18}$$

where n is the number of time steps of increment Δt and $\mathbf{u}_r = d\mathbf{u}_r/d\tau$.

C Effect of the History Force on the Mean Rise

To evaluate the impact of the history force, we examined the effect of different time intervals. Simulations with the Feng and Michaelides C_D , Kurose and Komori C_L , $C_{VM} = 1/2$, and using the Basset description of the history force

with time intervals of $\tilde{\tau}/\tilde{\tau}_\eta = \tau/\tau_\eta = 0.05, 0.1, 0.5, 1.0$ and 2.0 were performed, where $\tilde{\tau} \equiv n\Delta t$ and

$$\tilde{\tau}_\eta \equiv (\tilde{\nu}/\tilde{\epsilon})^{1/2} \quad (19)$$

refers to the Kolmogorov timescale³⁹. For the sake of completeness, Table 3 shows the normalized values of other time scales relevant to the present problem, namely: (a) the eddy turnover time:⁴⁰

$$\tilde{\tau}_0 = \tilde{l}_0/\tilde{u}_0 \quad (20)$$

where \tilde{l}_0 and \tilde{u}_0 are the characteristic eddy length and velocity scales; and (b) the droplet response time scale:⁴¹

$$\tilde{\tau}_d \equiv \frac{(2r_\rho + 1)}{9} \frac{\tilde{a}^2}{\tilde{\nu}_c} \quad (21)$$

where r_ρ is the ratio of droplet to fluid density.

Results of the simulation are shown in Figure 11, which depicts the predicted mean droplet rise for various diameters. The results indicate that increasing the time interval in the Basset integral has only a small effect on the computed mean rise of the droplets. Compared to the baseline simulation, droplets with smaller radii show slight retardation of rise while droplets with larger radii droplets show slight enhancement of the mean rise velocity. Again the results are not consistent with the behavior observed by Friedman and Katz. Consequently, one can conclude that the history force, as modeled in the simulation, does not significantly impact the behavior of the droplets nor does it provide a plausible mechanism for explaining the surprising behavior observed by Friedman and Katz. This conclusion is also consistent with recent simulations of Burton and Eaton,⁴² who showed that the history force has a negligible contribution to the behavior of particles in decaying homogeneous isotropic turbulence.

VI Numerical Experimentation in the Variation of the Coefficient of Drag

Substantial empirical evidence exists that the particle, bubble and/or droplet C_D can vary significantly with turbulence conditions. For example, it is well

documented that turbulence hastens the transition to a turbulent boundary layer, with a resultant rapid decrease in C_D below quiescent values. As the turbulent boundary layer grows, C_D then increases to well above quiescent values. This phenomenon is often referred to as the “drag crisis.” For spheres, Figure 12 depicts experimentally observed drag coefficients and illustrates how these can differ significantly, both enhancement and suppression, from the standard drag curve.

In addition to the Reynolds number based on the relative velocity, experimental evidence also indicates that the drag coefficient experienced by small particles in turbulent flows may also depend on two additional dimensionless groups. The first is the ratio (or inverse ratio) of the flow length scale to particle diameter, *i.e.* $\tilde{\eta}/\tilde{d}_p$ or $\tilde{d}_p/\tilde{\eta}$. For turbulent flows, the Kolmogorov length scale $\tilde{\eta}$ is widely used as the turbulence length scale. The second is the so-called relative turbulence intensity, I_r . Two definitions of I_r are frequently used in the literature, namely $I_r = \sqrt{u'^2}/|u_r|$ or $I_r = \sqrt{u'^2}/|u_t|$, where u' is r.m.s. velocity fluctuation, $|u_r|$ is the magnitude of the mean relative velocity between the particle and the turbulent flow, and $|u_t|$ is the magnitude of the particle terminal velocity in a quiescent fluid. We shall use the definition based on the terminal velocity. Figure 13 shows I_r versus droplet diameter for oil droplets considered in the present study, *i.e.* for turbulence conditions corresponding to Friedman and Katz large facility L3.

Below, we provide a review of relevant literature on the behavior of C_D in unsteady flows, and later exploit this background information as a guide for numerical experiments on the impact of variation in the drag coefficient on the droplet mean rise.

A Behavior of C_D at $I_r \lesssim 0.5$ and low Re_p ($\lesssim 600$)

Rudoff and Bachalo⁴³ studied the behavior of very small droplets dispersed in turbulent air generated in the wake of fixed cylinder. The droplets were 10-50 μm diameter with droplet density $\tilde{\rho}_d$ much larger than the carrier fluid density $\tilde{\rho}_c$, *i.e.* $\tilde{\rho}_d/\tilde{\rho}_c \gg 1$. In their experiments, I_r was $\lesssim 0.23$ and $Re_p \lesssim 40$. The drag coefficient was estimated using a force balance between pressure drag and inertial forces acting upon a decelerating droplet; velocities of the turbulent air were not measured. Their results showed that the estimated C_D for 10-30 μm diameter droplets is well below the quiescent sphere C_D (7), with the 10 μm droplets having the largest suppression. In the experiments of Rudoff and Bachalo,⁴³ the number density of droplets increased as diameter decreased, so that the potential impact of droplet-droplet interactions may become more significant for the smaller particles.

Experiments by Uhlherr and Sinclair⁴⁴ of 1/16 to 3/4 inch (1588 to 19050 μm) spheres in turbulent water and glycerol solutions showed that C_D was generally enhanced as I_r increased. Uhlherr and Sinclair proposed the following correla-

tion to describe their observations:

$$\left\{ \begin{array}{ll} C_D = \frac{162I_r^{1/3}}{Re_p} & Re_p < 50, \quad 0.05 < I_r < 0.5 \\ C_D = 4I_r + 0.133 \left(1 + \frac{150}{Re_p}\right)^{1.585} & 50 \leq Re_p < 700, \quad 0.07 < I_r < 0.5 \end{array} \right. \quad (22)$$

Figure 14 compares the correlations (22) of Uhlherr and Sinclair with the standard drag correlation (7).

A similar trend is reported in the numerical study by Yusof.⁴⁵ Specifically, for $I_r \approx 0.19$ and $Re_p=100$, the drag of large particles increased by approximately 45% with respect to the quiescent value.

However, contrary results were obtained by Rudoff *et al.*⁴⁶ who showed that the C_D of small droplets (10-50 μm) in turbulent air was unchanged from quiescent C_D for $I_r \leq 0.09$. The experimental setup was the same used by Rudoff and Bachalo,⁴³ but both low and high number droplet densities were evaluated. Again, for these experiments $\tilde{\rho}_d/\tilde{\rho}_c \gg 1$. The observed C_D was independent of droplet number density, though there was large data scatter for the 10 μm droplets, possibly indicating droplet to droplet interactions.

Likewise, experiments of Wu and Faith^{47;48} with 1200 to 5600 μm diameter spheres in low turbulence ($I_r \approx 0.04$ and $0.08 \leq \tilde{\eta}/\tilde{d}_p \leq 0.80$), with $135 \leq Re_p \leq 1560$, showed a maximum of 6% deviation between the experimentally measured C_D and the standard quasi-steady drag correlation.

Direct simulations of Bagchi and Balachandar³⁶ showed that the free-stream turbulence does not have a substantial effect on the mean drag of solid spheres, with $1.5 \tilde{\eta} \leq \tilde{d}_p \leq 10 \tilde{\eta}$, $60 \leq Re_p \leq 600$ and I_r of about 0.10-0.25. Similarly, Merle *et al.*,⁴⁹ using a large-eddy simulation, showed that the quasi-steady drag coefficient for bubbles with $Re_p = 500$ is insensitive to weak turbulence ($I_r \ll 1$).

B Behavior of C_D at $I_r \lesssim 0.5$ and high Re_p

Torobin and Gauvin⁵⁰ investigated the behavior of smooth spheres, with diameters ranging from 1590 to 3210 μm , at $Re_p \gtrsim 600$ and with I_r up to 0.45. Their results indicate that C_D for these spheres drop well below that of the standard drag curve. Torobin and Gauvin determined a relationship between I_r and the critical Reynolds number Re_c , the Reynolds number where the downward steeply sloped portion of the experimentally determined C_D curve (for a given I_r) intersects the drag value of 0.3. Their relationship is expressed as:

$$Re_c I_r^2 = 45 \quad (23)$$

Clamen and Gauvin⁵¹ further investigated this phenomenon when they studied 1590 to 25500 μm spheres at $Re_p \gtrsim 1000$ and $0.07 \leq I_r \leq 0.35$. They observed a similar reduction in C_D . They also note that, as Re_p increases beyond Re_c , C_D rapidly rises to well above the standard drag curve. Clamen

and Gauvin⁵¹ further defined the hypercritical Reynolds number Re^* , which occurs when C_D passes 0.3 upwards from the minimum observed C_D , and the transcritical Reynolds number Re^T , which occurs at the maximum value of C_D above the standard C_D curve. For the parameter range studied, Clamen and Gauvin⁵¹ proposed the following relationships for Re^* and Re^T :

$$I_r Re^* = 400 \quad (24)$$

$$I_r Re^T = 1040 \quad (25)$$

and for the variation in C_D as a function of Re_p and I_r :

$$C_D = \frac{3990}{(\log_{10} Re_p)^{6.1}} - \frac{4.47 \times 10^5}{I_r^{0.97} Re_p^{1.80}} \quad (26)$$

with $Re^* < Re_p < 3 \times 10^4$, $Re^* \gtrsim 2000$ and $0.07 \leq I_r \leq 0.35$.

Neve and Jaafar⁵² studied large spheres (0.145 to 1.15-cm diameter) in a thin turbulent jet, conditions which yield $0.10 \leq I_r \leq 0.15$ and $Re_p > 1000$. They also noted a rapid drop followed by an increase in C_D from that of the standard drag curve. Their results show similar C_D trends to the data of Torobin and Gauvin⁵⁰ and of Clamen and Gauvin⁵¹ for $Re_p > Re^T$.

Clift and Gauvin,⁵³ analyzing the results of Torobin and Gauvin⁵⁰ and Clamen and Gauvin,⁵¹ determined the following equations for Re_c , Re^* and Re^T that better fits the experimental data:

$$\begin{cases} \log_{10} Re_c = 5.477 - 15.8I_r & I_r \leq 0.15 \\ \log_{10} Re_c = 3.371 - 1.75I_r & I_r \geq 0.15 \end{cases} \quad (27)$$

$$\begin{cases} \log_{10} Re^* = 6.878 - 23.2I_r & I_r \leq 0.15 \\ \log_{10} Re^* = 3.663 - 1.80I_r & I_r \geq 0.15 \end{cases} \quad (28)$$

$$Re^T = Re^* \times 1.13 \frac{1}{0.45 + 20I_r} \quad I_r < 0.07 \quad (29)$$

Clift and Gauvin⁵³ also determined a C_D relation similar to that of Clamen and Gauvin,⁵¹ (26), but which better fits the experimental data:

$$C_D = 0.3 \left(\left[\frac{Re}{Re_c} \right]^{-3} + \left[\frac{Re}{Re^*} \right]^{0.45+20I_r} \right) \quad (30)$$

for $0.9 Re_c \leq Re \leq Re^*$ and $I_r \geq 0.07$.

Transition from a laminar boundary layer to a turbulent boundary layer is the process that is thought to cause this rapid drop and then rapid rise in C_D , respectively, to well below and then well above the standard drag curve. This phenomenon, which is often referred to as the drag crisis, has been extensively studied since the early results of Ahlborn,⁵⁴ who showed that this transition can occur at $Re_p \ll 2000$.

C Behavior of C_D at $I_r \gg 0.5$

Levins *et al.*⁵⁵ studied the behavior of small iron and aluminum spheres, with 80 and 90 μm diameters, in intense turbulence with $\tilde{\eta} \approx 50 \mu\text{m}$ and $14 \lesssim I_r \lesssim 32$. They concluded, due to significant reductions in settling velocities of both the iron and aluminum particles in turbulence as compared to quiescent conditions, that the sphere C_D was significantly increased due to turbulence. (The settling velocity of the iron particles was reduced by about 60% while that of aluminum particles was reduced by about 30%.) They also noted that, with particle diameter approximately twice the Kolmogorov length scale, the particles had the tendency to follow the fluid motion much more than was predicted by the particle equation of motion using steady state values of the drag coefficient. Table 4 shows that the Stokes number for both the iron and aluminum particles was $\ll 1$.

Schwartzberg and Treybal^{56;57} studied the behavior of plastic and marble spheres settling in water in a rapidly stirred tank with $I_r \gtrsim 1.4$. Table 5 shows the material properties of the spheres, relative turbulence intensities studied and the observed settling velocity normalized by the settling velocity in a still or unstirred tank. They noted a significant reduction in settling velocity of the particles in the stirred tank and concluded that enhanced drag due to turbulence appears to be the cause for most of the observed reduction in settling velocity. Table 4 shows that $St \ll 1$ for both the plastic and marble particles.

Different results were obtained in simulations of Wang and Maxey.⁶ Their computations showed an increase in settling rate of heavy particles of up to 50% in isotropic turbulence with $\approx 2.3 \leq I_r \leq 3.8$. However, unlike the experiments of Levins *et al.*⁵⁵ and Schwartzberg and Treybal,^{56;57} the particles studied were much smaller than the Kolmogorov microscale $\tilde{\eta}$. Wang and Maxey note that the mechanism for enhancement of settling velocity is the preferential sweeping of the heavy particles to regions of downward moving fluid. The resulting enhanced settling of heavy particles has also been observed by Fung,^{58;59} based on simulations results for particles with $\tilde{\rho}_p/\tilde{\rho}_c \gg 1$, but at low turbulence intensity $I_r \leq .085$.

Experimental results of Aliseda *et al.*,⁶⁰ for $\approx 30 \mu\text{m}$ water droplets in air, and of Yang and Shy,⁶¹ for small ($\leq 40 \mu\text{m}$) copper, glass and lead spheres in water, showed enhancement of settling velocities due to isotropic turbulence. Yang and Shy,⁶¹ for example, observed a maximum increase in settling velocity of $\approx 38\%$ for $40 \mu\text{m}$ glass spheres with $I_r \approx 2.7$. In both experiments, $\tilde{\rho}_p/\tilde{\rho}_c \gg 1$ and $\tilde{d}_p \ll \tilde{\eta}$, with maximum enhancement of settling occurring when the Stokes number $St = \tilde{\tau}_p/\tilde{\tau}_f \approx 1$.

Based upon the cited experimental data, and as shown in Table 4, parameters that determine whether there is enhancement or retardation of heavy particle settling in turbulence include the ratio of particle diameter to the Kolmogorov microscale and the ratio of particle density to carrier fluid density. Specifically, heavy particle settling is enhanced in turbulence when $\tilde{d}_p/\tilde{\eta} \ll 1$ and $\tilde{\rho}_p/\tilde{\rho}_c \gg 1$. Settling is retarded in turbulence when $\tilde{d}_p/\tilde{\eta} \gtrsim 1$. A related observation is that heavy particle settling is enhanced when the Stokes number (also reported in

Table 4) is not much smaller than 1.

D Behavior of C_D in Oscillating Flows

Though not directly applicable to the present conditions, the behavior of the drag force experienced by spheres in oscillating flows can provide insight into the variation of C_D in unsteady flows. Specifically, for oscillating flows one can define the relative oscillation intensity:

$$I_r^\omega \equiv \frac{\omega \mathbf{A}}{u_t} \quad (31)$$

where ω is the oscillation frequency, \mathbf{A} is the oscillation amplitude and u_t is the terminal velocity in quiescent flow conditions, and examine the dependence of C_D or I_r^ω . A brief review of relevant prior work is provided below.

Hwang⁶² constructed a simple analytical model of the time-averaged particle force balance equation to analyze the behavior of heavy particles settling in an oscillating flow. The particle force balance equation used included the fluid pressure gradient, the submerged weight of the particle, the drag force and added mass, but the lift and history forces were omitted. Hwang⁶² showed for a simple harmonic flow oscillation that the drag force on particles is significantly modified by the instantaneous relative velocity between the particles and surrounding fluid. His analytic solution also predicts that the settling velocity of heavy particles in fluid undergoing harmonic oscillations will be reduced when compared to settling in a still fluid.

Baird *et al.*⁶³ studied the behavior of large, 1/8 and 1/2 in. (3200 - 12700 μm) diameter, plastic spheres in water undergoing oscillations of 0.88 - 2.37 sec^{-1} with amplitudes of 1.1 - 4.0 in (3.6 - 10 cm). The density of plastic spheres was slightly greater than that of the carrier fluid ($\tilde{\rho}_p/\tilde{\rho}_c \approx 1.18$). For $0.68 \leq I_r^\omega \leq 0.92$, they observed a reduction in settling velocity of approximately 28% and concluded that the decrease in settling velocity is due to shedding of a large wake during each oscillation, and that $C_D(I_r^\omega > 0) > C_D(I_r^\omega = 0)$.

Similar results were obtained by Takahashi *et al.*⁶⁴ who studied large nickel-plated nylon balls falling in an oscillating water column with frequency 0.8 - 2.2 sec^{-1} and amplitude 1.36 - 4.06 cm. The balls were 8000 - 15900 μm diameter and $\tilde{\rho}_p/\tilde{\rho}_c \approx 1.3$. Their results for $I_r \lesssim .08$ showed a reduction of particle settling velocity of up to 26%; consequently, they concluded that $C_D(I_r^\omega > 0) > C_D(I_r^\omega = 0)$.

Tunstall and Houghton⁶⁵ studied both large (up to 0.505 cm) and small (208-833 μm) diameter sapphire and glass spheres in a vertically oscillating water column at 5 - 50 sec^{-1} and 0 - 1.0 cm amplitudes. For both the sapphire and glass spheres $\tilde{\rho}_p/\tilde{\rho}_c \gg 1$. The smallest spheres experienced $I_r^\omega \approx 13$, while the larger spheres had smaller intensities. The larger spheres exhibited reduced settling velocities, while smaller spheres exhibited higher than expected settling velocities. These results suggest that for larger spheres $C_D(I_r^\omega > 0) \gg C_D(I_r^\omega = 0)$, while for smaller spheres $C_D(I_r^\omega > 0) \ll C_D(I_r^\omega = 0)$.

It is instructive to evaluate the Stokes numbers corresponding to the data of Tunstall and Houghton.⁶⁵ For the largest particles studied, \tilde{d}_p of 5050 μm with $\tilde{\rho}_p/\tilde{\rho}_c \approx 2.6$, the particle relaxation time $\tilde{\tau}_p$ is ≈ 3.7 sec. For the smallest particles studied, \tilde{d}_p of 208 μm with $\tilde{\rho}_p/\tilde{\rho}_c \approx 2.5$, $\tilde{\tau}_p$ is ≈ 0.006 sec. Using $\tilde{\tau}_\omega = 1/\omega$ as the characteristic time scale of the oscillating field, one finds $St \gg 1$ for the largest particles, where $C_D(I_r^\omega > 0) \gg C_D(I_r^\omega = 0)$, and $St \ll 1$ or $St < 1$ for the smallest particles, where $C_D(I_r^\omega > 0) \ll C_D(I_r^\omega = 0)$.

The experimental results for heavy particles settling in oscillating flows is shown in Table 6. Comparison is made with Table 4 which shows similar properties for heavy particles settling in turbulent flow. There is no evident correlation between the ratios of length scales, *e.g.* $\tilde{d}_p/\tilde{\eta}$ and \tilde{d}_p/\mathbf{A} , and the observed enhancement or retardation of heavy particle settling.

E Variation in C_D with $\tilde{\eta}/\tilde{d}_p$

Magelli *et al.*⁶⁶ determined that the settling velocities of plastic, glass and bronze beads (140-980 μm diameter and $1.15 \leq \tilde{\rho}_p/\tilde{\rho}_c \leq 8.41$) were reduced in stirred versus unstirred tanks. They proposed that the reduction occurred due to interaction between the particles and turbulent field when $\tilde{\eta}/\tilde{d}_p < 0.1$ or $\tilde{d}_p/\tilde{\eta} > 10$. They observed a limiting value of approximately 0.4 for the ratio of stirred tank settling velocity to unstirred tank settling velocity, u_s/u_t , which occurred around $\tilde{\eta}/\tilde{d}_p \approx 0.05$.

Nocentini and Magelli¹⁰ observed the settling velocities of glass and plastic spherical beads in a continuously stirred water vessel. The glass beads ($\tilde{\rho}_p/\tilde{\rho}_c \approx 2.45$) were 330 μm diameter and the plastic beads ($\tilde{\rho}_p/\tilde{\rho}_c \approx 1.15$) were 230 μm diameter. As shown in Figure 4, Nocentini and Magelli determined the following correlations for u_s/u_t as a function of $\tilde{\eta}/\tilde{d}_p$ or $\tilde{d}_p/\tilde{\eta}$:

$$\left\{ \begin{array}{ll} \frac{u_s}{u_t} = 1 & \frac{\tilde{\eta}}{\tilde{d}_p} > 0.2 \quad \left[\frac{\tilde{d}_p}{\tilde{\eta}} > 5 \right] \\ \frac{u_s}{u_t} = 1.5 + \log_{10} \left(\frac{\tilde{\eta}}{\tilde{d}_p} \right) & .04 < \frac{\tilde{\eta}}{\tilde{d}_p} < 0.2 \quad \left[25 > \frac{\tilde{d}_p}{\tilde{\eta}} > 5 \right] \\ \frac{u_s}{u_t} = 0.5 & \frac{\tilde{\eta}}{\tilde{d}_p} < 4 \times 10^{-2} \quad \left[\frac{\tilde{d}_p}{\tilde{\eta}} > 25 \right] \end{array} \right. \quad (32)$$

Brucato *et al.*⁶⁷ studied the behavior of spherical glass beads ($\approx 70, 250$ and $500 \mu\text{m}$ diameter) and irregularly shaped silica particles (≈ 210 and $500 \mu\text{m}$ maximum dimension) settling in a Couette-Taylor flow field. The Couette-Taylor flow field was generated by rotating an interior cylinder inside a fixed exterior cylinder. At low rotational speeds the test apparatus produced laminar Couette flow, laminar Taylor flow, wavy vortex flow, etc. The highest rotational speeds studied produced fully turbulent flow with maximum $I_r < 0.5$. The bead and

particle density were approximately 2.5 times that of the carrier fluid. At the highest I_r they observed drag coefficients for the 500 μm beads approximately forty times greater than that in a still fluid. However, the 70 μm beads showed no significant change in settling velocity.

Brucato *et al.*⁶⁷ determined the following correlation for instantaneous drag coefficient C_D normalized by the drag coefficient in quiescent fluid C_{D_o} :

$$\frac{C_D - C_{D_o}}{C_{D_o}} = 8.76 \times 10^{-4} \left(\frac{\tilde{d}_p}{\tilde{\eta}} \right)^3 \quad (33)$$

This correlation results in C_D being larger than the quiescent fluid drag coefficient C_{D_o} when $\tilde{d}_p \gg \tilde{\eta}$. For example, a 500 μm diameter particle in a turbulent field with Kolmogorov length scale of 40 μm would have a $C_D = 2.71 C_{D_o}$ as follows:

$$\frac{C_D - C_{D_o}}{C_{D_o}} = 8.76 \times 10^{-4} \left(\frac{500 \mu\text{m}}{40 \mu\text{m}} \right)^3 \approx 1.71$$

and thus $C_D - C_{D_o} \approx 1.71 C_{D_o}$ or $C_D \approx 2.71 C_{D_o}$.

On the other hand, a 100 μm diameter particle in the same ($\tilde{\eta} = 40 \mu\text{m}$) turbulent field would have $C_D \approx C_{D_o}$. In this case,

$$\frac{C_D - C_{D_o}}{C_{D_o}} = 8.76 \times 10^{-4} \left(\frac{100 \mu\text{m}}{40 \mu\text{m}} \right)^3 \approx 0.0137$$

and thus $C_D - C_{D_o} \approx .0137 C_{D_o}$ or $C_D \approx 1.037 C_{D_o}$.

A summary of the experimentally observed dependences above of C_D on $\tilde{\eta}/\tilde{d}_p$ is provided in Table 7.

Burton and Eaton⁴² performed two-way coupling and fully resolved simulations of particle-turbulence interactions for a fixed particle in decaying homogeneous turbulence. The simulations commenced with $d_p \approx 2 \eta_K$ and $Re_p \approx 19$. (Since the particle was fixed and turbulence was decaying, estimation of I_r is not feasible.) The simulations showed that drag was the dominant force and that the particle equation of motion using the standard drag correlation (7) underestimated the root mean square forces on the particle by between 15 and 30%.

Finally, Torobin and Gauvin⁶⁸ showed that, in turbulence, very small particles ($\tilde{d}_p \lesssim 50 \mu\text{m}$) move at the local fluid velocity without appreciable relative motion. Consequently, and without relative velocity between the particles and the fluid, drag force is not generated. Lumley,⁶⁹ Chow and Saibel⁷⁰ and Clift and Gauvin⁵³ estimated that the particle diameter for this behavior must satisfy the following conditions:

$$\frac{\tilde{d}_p}{\tilde{\eta}} \ll 1, \quad (34)$$

$$Re_t = \frac{\tilde{d}_p u'}{\tilde{\nu}} \ll 1, \quad (35)$$

where Re_t is the turbulent Reynolds number of the particle, and

$$\frac{\tilde{d}_p^2}{9\tilde{\nu}} \left[2 \left(\frac{\tilde{\rho}_p}{\tilde{\rho}_c} \right) + 1 \right] \ll \frac{\tilde{\eta}^2}{\tilde{\nu}}, \quad (36)$$

or that the particle response time $\tilde{\tau}_p$, the left hand side of equation (36), is much smaller than the Kolmogorov time scale $\tilde{\tau}_\eta$, the right hand side of equation (36), such that the Stokes number $St = \tilde{\tau}_p/\tilde{\tau}_\eta \ll 1$.

F Summary of Behavior of C_D in Turbulent Flows

Based on the available experimental and computational observations discussed above, the following features can be identified of the behavior of C_D for heavy particles in turbulent flow.

1. For $I_r \lesssim 0.5$ there is no significant change in particle C_D with turbulence except for $Re_p \gtrsim 600$. When $Re_p \gtrsim 600$, the transition to a turbulent boundary layer and wake, sometimes referred to as the “drag crisis,” causes C_D to drop rapidly to ≈ 0.1 , followed by a rapid rise to well above the standard drag curve.
2. For $I_r \gg 0.5$ and for large particles ($\tilde{d}_p/\tilde{\eta} \geq 10$), particle C_D is enhanced by turbulence.
3. For $I_r \gg 0.5$ and for smaller particles ($1 - 2 < \tilde{d}_p/\tilde{\eta} < 10$), limited experimental data suggests that particle C_D may be reduced by turbulence.
4. For $I_r \gg 0.5$ and $\tilde{d}_p \ll \tilde{\eta}$, settling of heavy particles is enhanced due to preferential sweeping to down flow regions, particularly when $St \approx 1$.

G Effect of Variation of C_D on Droplet Mean Rise

The experimental results of Friedman and Katz reveal dramatically different behavior for droplets smaller than approximately 400 μm radii, which exhibit enhancement of rise in turbulence, while droplets larger than approximately 400 μm radii exhibit a suppression of the mean rise velocity. The “boundary” between these different behaviors occurs at droplet diameters approximately ten times the Kolmogorov length scale (*i.e.* $\tilde{d}_p \approx 10 \tilde{\eta}$). As discussed above, such behavior is consistent with the experimental trends for heavy particles settling in turbulence, for which C_D is reduced or enhanced by turbulence depending upon the ratio $\tilde{d}_p/\tilde{\eta}$. This observation suggests (and to certain extent justifies) numerical experimentation with varying the droplet C_D , particularly to assess whether variation inspired by experimental trends can help decrease the disparity between predicted and observed mean rise velocities.

Numerous modifications of droplet C_D in turbulence were considered in order to better approximate the experimental results of Friedman and Katz. Consistent with experimental observations summarized above, the analysis focused on modifications to droplet C_D based on turbulence intensity.

Attempts (not shown) to modify C_D based on the instantaneous relative turbulence intensity were unsuccessful in bringing significant improvement of simulation results compared with experimental data. Consequently, a modified droplet C_D was considered based upon the mean turbulence intensity

$$\bar{I}_r = \frac{\sqrt{\overline{u'^2}}}{\bar{u}_r} \quad (37)$$

where \bar{u}_r is the mean relative velocity for a given droplet diameter calculated in the baseline simulation (with Feng and Michaelides C_D , Kurose and Komori C_L , $C_{VM}=1/2$ and $C_H = 0$). Note that, in the baseline simulation, droplets with radii $\leq 400 \mu\text{m}$ had $\bar{I}_r \gtrsim 5$, $450 \mu\text{m}$ radius droplets had $\bar{I}_r \approx 5$ and droplets with radii $\geq 500 \mu\text{m}$ had $\bar{I}_r \lesssim 5$.

With a significantly enhanced C_D for $\bar{I}_r < 5.0$ and $\tilde{d}_p/\tilde{\eta} \geq 10$, and a significantly reduced C_D for $\bar{I}_r > 5.0$ and $\tilde{d}_p/\tilde{\eta} < 10$, the simulation was able to better approximate the observed experimental behavior for droplets with radius greater than $450 \mu\text{m}$ (*i.e.* suppression of rise rate in turbulence). However, the simulation was unable to capture the observed behavior for droplets with radius less than $450 \mu\text{m}$ (*i.e.* enhancement of rise rate in turbulence), even as $C_D \rightarrow 0$.

The most favorable agreement with experimental trends that we could obtain was based on the C_D correlation depicted in Figure 15. The correlation, which is inspired by some of the experimental trends reviewed earlier, is specified by:

1. $\bar{I}_r \gtrsim 5.0$:

$$\begin{cases} C_D = 0.005 + (0.0001 Re_d) & Re_d \leq 100 \\ C_D = 0.01 + 0.015074(Re_d - 100) & 100 < Re_d \leq 150 \\ C_D \Rightarrow \text{Feng and Michaelides } C_D & Re_d > 150 \end{cases} \quad (38)$$

2. $\bar{I}_r \approx 5.0$: Feng and Michaelides C_D was used,

3. $\bar{I}_r \lesssim 5.0$:

$$\begin{cases} C_D \Rightarrow \text{Feng and Michaelides } C_D & Re_d < 10 \\ C_D = 14.0 + 0.070(Re_d - 10) & Re_d \geq 10 \end{cases} \quad (39)$$

Plotted in Figure 16 are the droplet mean rise velocities obtained with the modified C_D correlation shown in Figure 15. For droplet radii larger than $400 \mu\text{m}$, the predictions are in good agreement with the experimental results of Friedman and Katz. In particular, in this range of droplet radii both the experiments and computations reveal substantial suppression of the rise velocity below the quiescent value. On the other hand, for droplet radii smaller than $350 \mu\text{m}$, significant discrepancies between the predictions and experimental results can still be observed. Specifically, the computations show these smaller droplets rising approximately at quiescent rise velocity, while the experimental results of Friedman and Katz clearly show that these droplets have mean rise velocities well above the corresponding quiescent values.

VII Numerical Experiments with Concurrent Variation of C_D and C_{VM}

The scope of the numerical experiments above is extended in this section by allowing for variation in the virtual mass coefficient.

Note that in all simulations above C_{VM} was set to $1/2$, namely the value determined for a sphere accelerating in a potential flow.¹⁹ The suitability of using this coefficient in various settings has received considerable attention. Early experiments by Lunnon⁷¹ of 0.238 to 5.08 cm steel, bronze and lead spheres ($7.75 \leq \tilde{\rho}_s/\tilde{\rho}_c \leq 10.5$) accelerating in otherwise still water showed that the “carried mass” (virtual mass) varied from $1/2$ to twice the mass of the displaced water. More recent analyses for both uniform and nonuniform flows, namely by Rivero *et al.*,⁷² Mei *et al.*,³² Mei and Klausner,⁷³ Chang and Maxey,⁷⁴ Magnaudet and Eames,⁷⁵ Balachandar,⁴¹ and others show that $C_{VM}=1/2$ is suitable for both bubbles and solid spheres, and is independent of the bubble or sphere Reynolds number, the temporal and convective acceleration of the carrier fluid, and whether a no-slip or shear-free boundary condition is present.

Unfortunately, there is little experimental data concerning the variation in C_{VM} in turbulence. Extrapolation of the analysis of Magnaudet and Eames⁷⁵, Balachandar⁴¹ and others suggests that C_{VM} is independent of I_r . This conclusion, however, is based on studies at low relative turbulence intensities ($I_r \lesssim .5$). The authors are unaware of any experimental measurement or analysis of C_{VM} at moderate or high turbulence intensities ($I_r \geq .5$).

On the other hand, well-established evidence exists that C_{VM} may vary in unsteady flows. For example, Odar and Hamilton⁷⁶ proposed that the virtual mass of a sphere in a harmonic flow depends on the acceleration parameter,

$$Ac = \frac{u_r^2}{\tilde{d}_p \frac{du_r}{dt}}, \quad (40)$$

where u_r is relative velocity of the sphere with respect to the flow, \tilde{d}_p is diameter of the sphere and du_r/dt is relative acceleration, and provided the following empirical correlation for a sphere in simple harmonic motion in the range $0 \leq Re_p \leq 62$:

$$C_{VM} = 2.1 - \frac{0.132}{0.12 + Ac^2} \quad (41)$$

In their observations of small (208-833 μm diameter) spheres in intense harmonic flows ($3.3 \lesssim I_r^\omega \lesssim 13$), Tunstall and Houghton⁶⁵ suggest that oscillation-induced variation in C_{VM} may, in addition to oscillation-induced variation in

C_D , play a role in the enhancement in the spheres' settling velocities. Specific parametrization of this effect, however, was not provided.

In the absence of well-established evidence on the behavior of C_{VM} for at moderate and large turbulence intensities, numerical experiments were conducted based on the postulate that both C_D and C_{VM} experience significant reductions at high \overline{T}_r and with $\tilde{d}_p/\tilde{\eta} \leq 10$. In particular, numerical experiments were performed with the turbulence modified C_D , (38) and (39), and with $C_{VM} \rightarrow 0$ as droplet radius becomes less than $450 \mu\text{m}$. Note that for the present turbulence conditions, a $450 \mu\text{m}$ radius corresponds to a ratio of $\tilde{d}_p/\tilde{\eta} = 10$; thus, the postulated transition is consistent with the experimental observations of Magelli *et al.*⁶⁶ and Nocentini and Magelli.¹⁰

Using an iterative refinement of the postulated behavior, close agreement can be obtained between the model predictions and the experimental results of Friedman and Katz. The most favorable agreement obtained was based on the C_{VM} depicted in Figure 17, with the corresponding mean rise velocities are shown in Figure 18.

It is interesting to note that the postulated suppression of C_{VM} for the smaller droplets lead to an appreciable change in mean rise predictions (and consequently to better agreement with the experimental predictions). This differs from experiences with bubbles or heavy particles at low turbulence intensities, in which the virtual mass force is small compared to the magnitude of the drag force, *e.g.* $|F_{VM}| \ll |F_D|$.¹⁷ In the present case, however, small slightly-buoyant droplets have small rise velocities while experiencing intense relative accelerations, and thus the magnitudes of the virtual mass and drag forces become comparable. This observation, which is readily verified from the computations, explains the otherwise peculiar impact on mean rise velocities.

VIII Conclusions

A simplified numerical study has been conducted in this paper of the puzzling experimental results of Friedman and Katz, which indicate that the mean rise of slightly-buoyant, small ($\tilde{d} < 800 \mu\text{m}$) droplets is larger in isotropic turbulence than in quiescent conditions, whereas the mean rise of larger droplets is suppressed. The computations specifically explore whether these experimental trends can be captured using a simplified one-way coupling model that combines DNS of the turbulent field with a Lagrangian dynamical equation describing the droplet motion.

Baseline values for the force coefficients appearing in the Lagrangian equation of motion of the bubbles are first defined, based on straightforward extension of previous analysis for bubbles in isotropic turbulence.⁸ In the baseline analysis, the coefficient of drag is adapted from the quasi-steady correlation of Feng and Michaelides⁹ for viscous droplets, the lift coefficient is adapted from the correlation of Kurose and Komori for particles in linear shear,²³ with the virtual mass coefficient $C_{VM} = 1/2$, and the history force coefficient $C_H = 0$, *i.e.* the history force is ignored. Computed results obtained with these baseline

coefficients indicate that, for the conditions of the experimental results of Friedman and Katz, there is a uniform suppression of the droplet mean rise velocity with respect to quiescent rise values. In particular, large discrepancies occur between the baseline predictions and the experimental data of Friedman and Katz, especially for small droplet diameters.

A numerical study was subsequently conducted in order to assess the impact of uncertainty or variability in individual force coefficients on the mean droplet rise predictions. Results of these numerical experiments indicate that, within a wide range of variability, the lift and history force coefficients have an insignificant impact on the mean rise predictions. In particular, the postulated variations are not able to resolve the discrepancies between the predicted mean rise velocities and the experimental observations.

Numerical experiments were also conducted to explore the impact of variability in the drag force coefficient on the droplet mean rise. These experiments were guided by empirical observations indicating that at high turbulence intensities, the drag coefficient of large ($\tilde{d}_p/\tilde{\eta} > 10$) particles can be significantly larger than the corresponding quasi-steady estimate, whereas the drag coefficient for particles with $\tilde{d}_p/\tilde{\eta}$ in the range 1-10 may be significantly suppressed. Using this postulate, the predictions exhibit reasonable agreement with the experimental values for droplets with radii larger than $350 \mu\text{m}$, but significantly under-predict the mean rise of smaller droplets. Finally, by postulating in addition that the coefficient of virtual mass of the smaller droplets is suppressed in a similar fashion to the drag coefficient, it is shown that the computed predictions exhibit a reasonable agreement with experimental results across the entire range of droplet sizes considered in the experiments.

The numerical analysis completed herein, with the surprising postulate that both the drag and virtual mass of smaller droplets in intense turbulence may be suppressed to insignificant values, assumes that a simplified one-way coupling model combined with a Lagrangian equation of motion can correctly capture the observed droplet behavior. While, in our prior work,⁸ the same model correctly predicted the behavior of small bubbles in intense turbulence, the force correlations used therein were based upon a large collection of experimental data for individual correlations. In this study, however, the experimental data is limited to droplet rise rates in turbulence, with no independent experimental data for validation of individual force correlations used.

A possible physical explanation for the postulated rapid decrease in C_D and C_{VM} is that the rapidly changing and intense turbulent flow does not allow for the formation of a significant wake behind the small oil droplets, which have minimal buoyancy to promote relative movement with respect to the turbulent flow. Without a significant wake the small oil droplets would experience minimal form drag, with C_D and C_{VM} thus tending to zero.

The present experiences underscore several difficulties in modeling the motion of small particles under high turbulence intensities. Specifically, they clearly demonstrate that straightforward extrapolation of methodologies established under low turbulence intensities can lead to large predictive errors. For the conditions considered in the present study, these errors could be effectively min-

imized by postulating modification of the drag and added mass coefficients. However, though the postulated modifications are consistent with experimental trends, a well-established fundamental basis for their implementation is still lacking. Additional work is currently planned to further explore their validity, based on exploiting extensive experimental data on droplet dispersion, and on complementing dispersion analysis with direct numerical simulations for relevant turbulence conditions.

References

- ¹ P.D. Friedman and J. Katz. Mean rise rate of droplets in isotropic turbulence. *Physics of Fluids*, 14(9):3059–3073, 2002.
- ² L.P. Wang and M.R. Maxey. The motion of microbubbles in a forced isotropic and homogeneous turbulence. *Applied Science Research*, 51:291–296, 1993a.
- ³ P.D.M. Spelt and A. Biesheuvel. On the motion of gas bubbles in homogeneous isotropic turbulence. *Journal of Fluid Mechanics*, 336:221–244, 1997.
- ⁴ R.E.G. Poorte and A. Biesheuvel. Experiments on the motion of gas bubbles in turbulence generated by an active grid. *Journal of Fluid Mechanics*, 461:127–154, 2002.
- ⁵ M.R. Maxey. The gravitational settling of aerosol particles in homogeneous turbulence and random flow fields. *Journal of Fluid Mechanics*, 174:441–465, 1987.
- ⁶ L.P. Wang and M.R. Maxey. Settling velocity and concentration distribution of heavy particles in homogeneous isotropic turbulence. *Journal of Fluid Mechanics*, 256:27–68, 1993b.
- ⁷ R. Mei. Flow due to an oscillating sphere and an expression for unsteady drag on the sphere at finite reynolds number. *Journal of Fluid Mechanics*, 270:133–174, 1994.
- ⁸ M.R. Snyder, O.M. Knio, Joseph Katz, and O.P. Le Maître. Statistical analysis of small bubble dynamics in isotropic turbulence. *Physics of Fluids*, 19:065108, 2007.
- ⁹ Z-G. Feng and E.E. Michaelides. Drag coefficients of viscous spheres at intermediate and high reynolds numbers. *Transactions of the ASME: Journal of Fluids Engineering*, 123:841–849, 2001.
- ¹⁰ M. Nocentini and F. Magelli. Solid distribution in slurry reactors stirred with multiple impellers: continuous flow systems. *7th European Conference on Mixing, 18–20 September 1991, Brugge, Belgium; proceedings*, pages 461–468, 1991.
- ¹¹ S. Elghobashi. On predicting particle-laden turbulent flows. *Applied Scientific Research*, 52:309–329, 1994.
- ¹² E. Loth. Numerical approaches for motion of dispersed particles, droplets and bubbles. *Progress in Energy and Combustion Science*, 26:161–223, 2000.
- ¹³ S. Cerutti, O. Knio, and J. Katz. Numerical study of cavitation inception in the near field of an axisymmetric jet at high reynolds number. *Physics of Fluids*, 12:2444–2460, 2000.

- ¹⁴ A.M. Ahmed and S. Elghobashi. Direct numerical simulation of particle dispersion in homogeneous turbulent shear flows. *Physics of Fluids*, 13:3346–3364, 2001.
- ¹⁵ M.R. Snyder. *Analysis of the behavior of bubbles and droplets in isotropic turbulence*. PhD thesis, The Johns Hopkins University, Baltimore, 2007.
- ¹⁶ M.R. Maxey and J.J. Riley. Equation of motion for a small rigid sphere in a nonuniform flow. *Physics of Fluids*, 26:883–889, 1983.
- ¹⁷ G. Sridhar and J. Katz. Drag and lift forces on microscopic bubbles entrained by a vortex. *Physics of Fluids*, 7:389–399, 1995.
- ¹⁸ G. Sridhar and J. Katz. Effect of entrained bubbles on the structure of vortex rings. *Journal of Fluid Mechanics*, 397:171–202, 1999.
- ¹⁹ C. Crowe, M. Sommerfeld, and Y. Tsuji. *Multiphase Flows with Droplets and Particles*. CRC, Boca Raton, 1998.
- ²⁰ S. Winnikow and B.T. Chao. Droplet motion in purified systems. *Physics of Fluids*, 9:50–61, 1966.
- ²¹ J.F. Harper. The motion of bubbles and drops through liquids. *Advances in Applied Mechanics*, 12:59–129, 1972.
- ²² L.G. Leal. *Laminar Flow and Convective Transport Processes*. Butterworth-Heinemann, Boston, 1992.
- ²³ R. Kurose and S. Komori. Drag and lift forces on a rotating sphere in a linear shear flow. *Journal of Fluid Mechanics*, 384:183–206, 1999.
- ²⁴ G. Magnus. *On the deviation of projectiles; and on a remarkable phenomenon of rotating bodies*. Memoirs of the Royal Academy, Berlin, 1852.
- ²⁵ P.D.M. Spelt and A. Biesheuvel. Dispersion of gas bubbles in large-scale homogeneous isotropic turbulence. *Applied Scientific Research*, 58:463–482, 1998.
- ²⁶ I.M. Mazzitelli and D. Lohse. Lagrangian statistics for fluid particles and bubbles in turbulence. *New Journal of Physics*, 6:203, 2004.
- ²⁷ P. Bagchi and S. Balachandar. Effect of turbulence on the drag and lift of a particle. *Physics of Fluids*, 15:3496–3513, 2003.
- ²⁸ A.B. Basset. *A Treatise on Hydrodynamics*. Dover, New York, 1888.
- ²⁹ M.W. Reeks and S. McKee. The dispersive effects of basset history forces on particle motion in a turbulent flow. *Physics of Fluids*, 27:1573–1582, 1984.
- ³⁰ S. Yang and L.G. Leal. A note on memory-integral contributions to the force on an accelerating spherical drop at low reynolds number. *Physics of Fluids A: Fluid Dynamics*, 3:1822–1823, 1991.

- ³¹ P.M. Lovalenti and J.F. Brady. The force on a bubble, drop or particle in arbitrary time-dependent motion at small reynolds number. *Physics of Fluids A: Fluid Dynamics*, 5:2104–2116, 1993.
- ³² R. Mei, C.J. Lawrence, and R.J. Adrian. Unsteady drag on a sphere at finite reynolds number with small fluctuations in the free-stream velocity. *Journal of Fluid Mechanics*, 233:613–631, 1991.
- ³³ P.M. Lovalenti and J.F. Brady. The hydrodynamic force on a rigid particle undergoing arbitrary time-dependent motion at small reynolds number. *Journal of Fluid Mechanics*, 256:561–605, 1993.
- ³⁴ C.J. Lawrence and R. Mei. Long-time behaviour of the drag on a body in impulsive motion. *Journal of Fluid Mechanics*, 283:307–327, 1995.
- ³⁵ I. Kim, S. Elghobashi, and W.A. Sirignano. On the equation for spherical-particle motion: effect of reynolds and acceleration numbers. *Journal of Fluid Mechanics*, 367:221–253, 1998.
- ³⁶ P. Bagchi and S. Balachandar. Inertial and viscous forces on a rigid sphere in straining flows at moderate reynolds numbers. *Journal of Fluid Mechanics*, 481:105–148, 2003.
- ³⁷ I.S. Berezin and N.P. Zhidkov. *Computing Methods, Volume 1*. Addison-Wesley, Reading, Massachusetts, 1965.
- ³⁸ J.N. Chung. The motion of particles inside a droplet. *ASME C: Journal of Heat Transfer*, 104:438–445, 1982.
- ³⁹ A.N. Kolmogorov. Dissipation of energy in locally isotropic turbulence. *Dokl. Akad. Nauk SSSR*, 32:19–21, 1941.
- ⁴⁰ S.A. Pope. *Turbulent Flows*. Cambridge University Press, Cambridge, 2000.
- ⁴¹ S. Balachandar. Parameterization of force on a particle/bubble/droplet. *Multiphase Science and Technology*, 15:157–171, 2003.
- ⁴² T. Burton and J. Eaton. Fully resolved simulations of particle-turbulence interaction. *Journal of Fluid Mechanics*, 545:67–111, 2005.
- ⁴³ R.C. Rudoff and W.D. Bachalo. Measurements of droplet drag coefficients in a polydispersed turbulent flow field. *American Institute of Aeronautics and Astronautics Paper 88-0235*, pages 1–8, 1988.
- ⁴⁴ P.H.T. Uhlherr and C.G. Sinclair. The effect of free-stream turbulence on the drag coefficient of spheres. *Chemeca '70*, 1:1–13, 1970.
- ⁴⁵ J. Yusof. *Interaction of massive particles with turbulence*. PhD thesis, Cornell University, 1996.

- ⁴⁶ R.C. Rudoff and W.D. Kamemoto, D.Y. Bachalo. Effects of turbulence and number density on the drag coefficient of droplets. *American Institute of Aeronautics and Astronautics Paper 91-0074*, pages 1–7, 1991.
- ⁴⁷ J.-S. Wu and G.M. Faeth. Sphere wakes at moderate reynolds numbers in a turbulent environment. *American Institute of Aeronautics and Astronautics Journal*, 32:535–541, 1994.
- ⁴⁸ J.-S. Wu and G.M. Faeth. Effect of ambient turbulence intensity on sphere wakes at intermediate reynolds numbers. *American Institute of Aeronautics and Astronautics Journal*, 33:171–173, 1994.
- ⁴⁹ A. Merle, D. Legendre, and J. Magnaudet. Forces on a high-reynolds-number spherical bubble in a turbulent flow. *Journal of Fluid Mechanics*, 532:53–62, 2005.
- ⁵⁰ L.B. Torobin and W.H. Gauvin. The drag coefficients of single spheres moving in steady and accelerated motion in a turbulent field. *American Institute of Chemical Engineers Journal*, 7:615–619, 1961.
- ⁵¹ A. Clamen and W.H. Gauvin. Effects of turbulence on the drag coefficients of spheres in a supercritical flow regime. *American Institute of Chemical Engineers Journal*, 15:184–189, 1969.
- ⁵² R.S. Neve and F.B. Jaafar. The effects of turbulence and surface roughness on the drag of spheres in thin jets. *The Aeronautical Journal*, 86:3331–336, 1982.
- ⁵³ R. Clift and W.H. Gauvin. The motion of particles in turbulent gas streams. *Chemeca '70*, 1:14–28, 1970.
- ⁵⁴ V.F. Ahlborn. Turbulenz und mechanismus des widerstandes an kugeln und zylindern. *Zeitschr. Fur Technische Physik*, 10:482–491, 1931. German.
- ⁵⁵ D.M. Levins and J.R. Glastonbury. Particle-liquid hydrodynamics and mass transfer in a stirred vessel. part i—particle-liquid motion. *Transactions Institute Chemical Engineers*, 50:32–41, 1972.
- ⁵⁶ H.G. Schwartzberg and R.E. Treybal. Fluid and particle motion in turbulent stirred tanks: Fluid motion. *Industrial and Engineering Chemistry Fundamentals*, 7:1–6, 1968a.
- ⁵⁷ H.G. Schwartzberg and R.E. Treybal. Fluid and particle motion in turbulent stirred tanks: Particle motion. *Industrial and Engineering Chemistry Fundamentals*, 7:6–12, 1968b.
- ⁵⁸ J.C.H. Fung. Gravitational settling of particles and bubbles in homogeneous turbulence. *Journal of Geophysical Research*, 98:20287–20297, 1993.

- ⁵⁹ J.C.H. Fung. Effect of nonlinear drag on the settling velocity of particles in homogeneous isotropic turbulence. *Journal of Geophysical Research*, 103:27905–27917, 1998.
- ⁶⁰ A. Aliseda, A. Cartellier, F. Hainaux, and J.C. Lasheras. Effect of preferential concentration on the settling velocity of heavy particles in homogenous isotropic turbulence. *Journal of Fluid Mechanics*, 468:77–105, 2002.
- ⁶¹ T.S. Yang and S.S. Shy. Two-way interaction between solid particles and homogeneous air turbulence: particle settling rate and turbulence modification measurements. *Journal of Fluid Mechanics*, 526:171–216, 2005.
- ⁶² P.A. Hwang. Fall velocity of particles in oscillating flow. *Journal of Hydraulic Engineering*, 111:485–502, 1985.
- ⁶³ M.H.I. Baird, M.G. Senior, and R.J. Thompson. Terminal velocities of spherical particles in a vertically oscillating liquid. *Chemical Engineering Science*, 22:551–558, 1967.
- ⁶⁴ K. Takahashi, H. Miyazaki, S. Mori, and A. Tanimoto. Falling velocity of a particle in a sinusoidally oscillating fluid. *International Chemical Engineering*, 34:420–427, 1994.
- ⁶⁵ E.B. Tunstall and G. Houghton. Retardation of falling spheres by hydrodynamic oscillations. *Chemical Engineering Science*, 23:1067–1081, 1968.
- ⁶⁶ F. Magelli, D. Fajner, M. Nocentini, and G. Pasquali. Solid distribution in vessels stirred with multiple impellers. *Chemical Engineering Science*, 45:615–625, 1990.
- ⁶⁷ A. Brucato, F. Grisafi, and G. Montante. Particle drag coefficients in turbulent fluids. *Chemical Engineering Science*, 53(18):3295–3314, 1998.
- ⁶⁸ L.B. Torobin and W.H. Gauvin. Fundamental aspects of solids-gas flow. part vi: Multiparticle behavior in turbulent fluids. *The Canadian Journal of Chemical Engineering*, 39:113–120, 1961.
- ⁶⁹ J.L. Lumley. *Some problems connected with the motion of small particles in turbulent fluid*. PhD thesis, Johns Hopkins University, Baltimore, Maryland, 1957.
- ⁷⁰ P.L. Chow and E. Saibel. Some non-newtonian effects on the decay of isotropic turbulence. *International Journal of Engineering Science*, 5:723–739, 1967.
- ⁷¹ R.G. Lunnon. Fluid resistance to moving spheres. *Proceedings of the Royal Society of London. Series A, Containing Papers of a Mathematical and Physical Character*, 118(780):680–694, 1928.

- ⁷² M. Rivero, Magnaudet J., and Fabre J. Quelques résultats nouveaux concernant les forces exercées sur une inclusion sphérique par un écoulement accéléré. *C.R. Acad. Sci Paris Série II*, 312:1499–1506, 1991.
- ⁷³ R. Mei and J.F. Klausner. Unsteady force on a spherical bubble at finite reynolds number with small fluctuations in the free-stream velocity. *Physics of Fluids A*, 4:63–70, 1992.
- ⁷⁴ E.J. Chang and M.R. Maxey. Unsteady flow about a sphere at low to moderate reynolds number. part 2. accelerated motion. *Journal of Fluid Mechanics*, 303:133–153, 1995.
- ⁷⁵ J. Magnaudet and I. Eames. The motion of high-reynolds-number bubbles in inhomogeneous flows. *Annual Review of Fluid Mechanics*, 32:659–708, 2000.
- ⁷⁶ F. Odar and W. Hamilton. Forces on a sphere acceleration in a viscous flow. *Journal of Fluid Mechanics*, 18:302–314, 1964.

List of Tables

1	Turbulent Field Modeled. \tilde{L} is the side length of the domain, L^c is the characteristic length scale, U^c is the characteristic velocity, $t^c \equiv L^c/U^c$ is the characteristic time scale, $\tilde{t}_K = \sqrt{\tilde{\nu}/\tilde{\epsilon}}$ is the Kolmogorov time scale, $\tilde{t}_L = \tilde{t}_K Re^{1/2}$ is the integral time scale, $\tilde{\eta}$ is the Kolmogorov microscale, $\tilde{\lambda} = \sqrt{15\tilde{\nu}u'^2/\tilde{\epsilon}}$ is the Taylor length scale, and $\tilde{\epsilon}$ is the dissipation rate.	39
2	Simulation results using Feng and Michaelides (Ref. 9) C_D and Kurose and Komori (Ref. 23) C_L . $L_{z,min}$, $L_{z,max}$, $\langle L_z \rangle$ and $\langle L_{x,y,z} \rangle$ are, respectively, minimum lift force in the vertical direction, maximum lift force in the vertical direction, mean lift force in the vertical direction, and total lift force (all in Newtons). $\langle L_z \rangle / \langle D \rangle $ is mean lift force in the vertical direction normalized by magnitude of mean drag force. $\langle L_{x,y,z} \rangle / \langle D \rangle $ is mean lift force normalized by magnitude of mean drag force.	40
3	Normalized time scales (value for τ_d calculated for 300 μm radii droplets).	41
4	Experimentally observed behavior and Stokes number St for heavy particles experiencing relative turbulence intensity $I_r \gg 0.5$. \tilde{d}_p is particle diameter, $\tilde{\eta}_K$ is Kolmogorov microscale, $\tilde{\rho}_p$ is particle density and $\tilde{\rho}_c$ is carrier fluid density.	42
5	Properties and observed behavior of plastic and marble spheres settling in a stirred tank under high I_r (Schwartzberg and Treybal Ref. 57). \tilde{d}_p is particle diameter, $\tilde{\rho}_p$ is particle density, $\tilde{\rho}_c$ is carrier fluid density, I_r is relative turbulence intensity, u_s is settling velocity in a stirred tank and u_t is settling velocity in a still tank.	43
6	Experimentally observed behavior and Stokes number St for heavy particles in oscillating flows. \tilde{d}_p is particle diameter, \mathbf{A} is oscillation amplitude, $\tilde{\rho}_p$ is particle density, $\tilde{\rho}_c$ is carrier fluid density and I_r^w is the relative oscillation intensity.	44
7	Experimentally observed behavior for heavy particles versus $\tilde{d}_p/\tilde{\eta}_K$ or $\tilde{\eta}_K/\tilde{d}_p$. \tilde{d}_p is particle diameter, $\tilde{\rho}_p$ is particle density, $\tilde{\rho}_c$ is carrier fluid density, I_r is relative turbulence intensity, u_s is stirred tank settling velocity, u_t is unstirred tank settling velocity and $\tilde{\eta}_K$ is Kolmogorov microscale. (Note: I_r estimated from $\tilde{\eta}_K$.) . . .	45

List of Figures

1	Friedman and Katz (Ref. 1) experimentally determined quiescent rise velocity for slightly buoyant oil droplets. “Analysis fuel” refers to slightly buoyant fuel oil. Used with permission.	46
2	Friedman and Katz (Ref. 1) large facility L3 experimentally determined turbulent rise velocity, normalized by quiescent rise velocity, for slightly buoyant oil droplets in isotropic turbulence. Histogram reference to right scale shows number of droplets in analysis bin of 0.01 mm. Data points, \diamond , referenced to left scale show mean rise rate. Used with permission.	47
3	Friedman and Katz (Ref. 1) experimentally determined turbulence rise data for slightly buoyant oil droplets in large facility L3 compared with quiescent rise approximation using Feng and Michaelides (Ref. 9) C_D with viscosity ratio of 6.41. Upper horizontal scale shows droplet diameter normalized by Kolmogorov microscale, d_p/η_K	48
4	Stirred tank settling velocity normalized by unstirred tank settling velocity, u_s/u_t , versus Kolmogorov microscale normalized by particle diameter, η_K/d_p (Nocentini and Magelli Ref. 10). Upper horizontal scale shows particle diameter normalized by Kolmogorov microscale, d_p/η_K	49
5	Friedman and Katz (Ref. 1) experimentally determined quiescent rise data for slightly buoyant oil droplets compared with numerical approximation using Feng and Michaelides (Ref. 9) C_D	50
6	Standard sphere C_D and Feng and Michaelides (Ref. 9) C_D for fuel oil in water versus Reynolds number.	51
7	Kurose and Komori (adapted from Ref. 23) lift coefficient C_L for a stationary sphere in linear shear flow: $\triangle, \alpha^* = 0.1$; $\square, \alpha^* = 0.2$; $\diamond, \alpha^* = 0.3$; $\nabla, \alpha^* = 0.4$. α^* is dimensionless shear.	52
8	Friedman and Katz (Ref. 1) experimentally determined turbulence rise data for slightly buoyant oil droplets compared with baseline numerical approximation using Feng and Michaelides (Ref. 9) C_D and Kurose and Komori (Ref. 23) C_L . Upper horizontal scale shows droplet diameter normalized by Kolmogorov microscale, d_p/η_K	53
9	Simulation results for various combinations of lift and drag coefficients compared with experimental turbulent rise results of Friedman and Katz (Ref. 1). Upper horizontal scale shows droplet diameter normalized by Kolmogorov microscale, d_p/η_K	54
10	Probability density functions of the droplet lift force in the vertical direction, L_z , versus droplet radius.	55

11	Simulation results for Basset force with time history of $\tau/\tau_\eta=0.05$, 0.1, 0.5, 1.0, and 2.0 compared with experimental turbulent rise results of Friedman and Katz (Ref. 1). τ_η is Kolmogorov time scale. All simulations used Feng and Michaelides (Ref. 9) C_D , Kurose and Komori (Ref. 23) C_L and $C_{VM} = 1/2$. Upper horizontal scale shows droplet diameter normalized by Kolmogorov microscale, d_p/η_K	56
12	Standard drag curve and selected experimental drag curves for relative turbulence intensity $I_r > 0$ (adapted from Crowe <i>et al.</i> Ref. 19).	57
13	I_r based on relative and terminal droplet velocity versus oil droplet diameter for simulation of Friedman and Katz (Ref. 1) large facility L3 with $\hat{\eta} \approx 88 \mu m$. Upper horizontal scale shows droplet diameter normalized by Kolmogorov microscale, d_p/η_K	58
14	Variation in C_D versus Re_p and I_r following Uhlherr and Sinclair (Ref. 44).	59
15	Modified C_D correlations used versus Re_d and mean turbulence intensity \bar{I}_r	60
16	Simulation results for variation in C_D due to mean turbulence intensity \bar{I}_r compared with experimental turbulent rise results of Friedman and Katz (Ref. 1). Upper horizontal scale shows droplet diameter normalized by Kolmogorov microscale, d_p/η_K	61
17	Modified C_{VM} used versus droplet radius. Upper horizontal scale shows droplet diameter normalized by Kolmogorov microscale, d_p/η_K	62
18	Simulation results for variation in C_D and C_{VM} due to mean turbulence intensity \bar{I}_r compared with experimental turbulent rise results of Friedman and Katz (Ref. 1). Modified C_{VM} is that shown in Figure 17. Upper horizontal scale shows droplet diameter normalized by Kolmogorov microscale, d_p/η_K	63

\tilde{L} (m)	0.0250
L^c (m)	0.00398
U^c (m/s)	0.251
t^c (s)	0.0159
\tilde{t}_K (s)	0.00791
\tilde{t}_L (s)	0.250
$\tilde{\eta}$ (μm)	88
$\tilde{\lambda}$ (μm)	1650
$\tilde{\epsilon}$ (m^2/s^3)	0.016

Table 1: Turbulent Field Modeled. \tilde{L} is the side length of the domain, L^c is the characteristic length scale, U^c is the characteristic velocity, $t^c \equiv L^c/U^c$ is the characteristic time scale, $\tilde{t}_K = \sqrt{\tilde{\nu}/\tilde{\epsilon}}$ is the Kolmogorov time scale, $\tilde{t}_L = \tilde{t}_K Re^{1/2}$ is the integral time scale, $\tilde{\eta}$ is the Kolmogorov microscale, $\tilde{\lambda} = \sqrt{15\tilde{\nu}u'^2/\tilde{\epsilon}}$ is the Taylor length scale, and $\tilde{\epsilon}$ is the dissipation rate.

Radius μm	$L_{z,min}$ N	$L_{z,max}$ N	$\langle L_z \rangle$ N	$\langle L_{x,y,z} \rangle$ N	$\frac{\langle L_z \rangle}{ \langle D \rangle }$	$\frac{\langle L_{x,y,z} \rangle}{ \langle D \rangle }$
100	-3.678E-7	3.633E-7	-2.900E-11	6.303E-11	-0.0014	0.0031
200	-1.897E-6	1.468E-6	3.265E-9	3.281E-9	0.0196	0.0197
300	-3.698E-6	3.593E-6	2.431E-8	2.431E-8	0.0477	0.0447
400	-6.922E-6	5.883E-6	6.218E-8	6.219E-8	0.0502	0.0502
500	-1.917E-5	1.306E-5	9.778E-8	9.779E-8	0.0418	0.0418
600	-2.364E-5	2.579E-5	1.039E-7	1.039E-7	0.0267	0.0267
700	-6.636E-5	9.214E-5	2.455E-8	2.463E-8	0.0041	0.0041

Table 2: Simulation results using Feng and Michaelides (Ref. 9) C_D and Kurose and Komori (Ref. 23) C_L . $L_{z,min}$, $L_{z,max}$, $\langle L_z \rangle$ and $\langle L_{x,y,z} \rangle$ are, respectively, minimum lift force in the vertical direction, maximum lift force in the vertical direction, mean lift force in the vertical direction, and total lift force (all in Newtons). $\langle L_z \rangle / |\langle D \rangle|$ is mean lift force in the vertical direction normalized by magnitude of mean drag force. $\langle L_{x,y,z} \rangle / |\langle D \rangle|$ is mean lift force normalized by magnitude of mean drag force.

Time Scale	Symbol	Normalized Value
Eddy Turnover Time	τ_0	11.5
Droplet Response Time	τ_d	1.71
Kolmogorov Time Scale	τ_η	0.50

Table 3: Normalized time scales (value for τ_d calculated for 300 μm radii droplets).

	Levins <i>et al.</i> (Ref. 55)	Schwartzberg & Treybal (Ref. 57)	Aliseda <i>et al.</i> (Ref. 60)	Yang & Shy (Ref. 61)
\tilde{d}_p (μm)	80-90	540-5900	≈ 30	12-40
$\tilde{\eta}_K$ (μm)	50	≈ 33	210-273	350-460
$\tilde{d}_p/\tilde{\eta}_K$	≈ 1.7	$\gg 1$	$\ll 1$	$\ll 1$
$\tilde{\rho}_p/\tilde{\rho}_c$	2.69-7.28	1.11-2.85	$\gg 1$	$\gg 1$
I_r	$\approx 14-32$	$\gtrsim 1.4$	≈ 2.7	7.3-8.1
$St = \tau_p/\tau_f$	$\ll 1$	$\ll 1$	≈ 1	≈ 1
Observed Behavior	settling reduced	settling reduced	settling enhanced	settling enhanced
Proposed Mechanism	$C_D(I_r > 0) \gg$ $C_D(I_r = 0)$	$C_D(I_r > 0) \gg$ $C_D(I_r = 0)$	preferential sweeping to \downarrow flow regions	preferential sweeping to \downarrow flow regions

Table 4: Experimentally observed behavior and Stokes number St for heavy particles experiencing relative turbulence intensity $I_r \gg 0.5$. \tilde{d}_p is particle diameter, $\tilde{\eta}_K$ is Kolmogorov microscale, $\tilde{\rho}_p$ is particle density and $\tilde{\rho}_c$ is carrier fluid density.

	Resin	Lucite	Marble
\tilde{d}_p (μm)	540	5900	1100
$\tilde{\rho}_p/\tilde{\rho}_c$	1.11	1.18	2.85
I_r	2.5	3.0	1.4
u_s/u_t	0.40	0.28	0.43

Table 5: Properties and observed behavior of plastic and marble spheres settling in a stirred tank under high I_r (Schwartzberg and Treybal Ref. 57). \tilde{d}_p is particle diameter, $\tilde{\rho}_p$ is particle density, $\tilde{\rho}_c$ is carrier fluid density, I_r is relative turbulence intensity, u_s is settling velocity in a stirred tank and u_t is settling velocity in a still tank.

	Baird <i>et al.</i> (Ref. 63)	Takahashi <i>et al.</i> (Ref. 64)	Tunstall & Houghton (Ref. 65)	Tunstall & Houghton (Ref. 65)
\tilde{d}_p (μm)	3200-12700	8000-15900	5050	208-833
\mathbf{A} (μm)	102000	40600	10000	10000
\tilde{d}_p/\mathbf{A}	$\ll 1$	< 1	≈ 0.5	$\lesssim 0.0833$
$\tilde{\rho}_p/\tilde{\rho}_c$	1.18	1.3	2.6	2.5-4.0
I_r^ω	0.68-0.92	$\lesssim 0.08$	$\lesssim 0.83$	3.3-13
$St = \tau_p/\tau_f$	$O(10)$	$O(40)$	$O(30)$	$O(0.5)$ - $O(5)$
Observed Behavior	settling reduced	settling reduced	settling reduced	settling enhanced
Proposed Mechanism	$C_D(I_r^\omega > 0) \gg$ $C_D(I_r^\omega = 0)$	$C_D(I_r^\omega > 0) \gg$ $C_D(I_r^\omega = 0)$	$C_D(I_r^\omega > 0) \gg$ $C_D(I_r^\omega = 0)$	$C_D(I_r^\omega > 0) \ll$ $C_D(I_r^\omega = 0)$

Table 6: Experimentally observed behavior and Stokes number St for heavy particles in oscillating flows. \tilde{d}_p is particle diameter, \mathbf{A} is oscillation amplitude, $\tilde{\rho}_p$ is particle density, $\tilde{\rho}_c$ is carrier fluid density and I_r^ω is the relative oscillation intensity.

	Magelli <i>et al.</i> (Ref. 66)	Nocentini & Magelli (Ref. 10)	Brucato <i>et al.</i> (Ref. 67)
Flow	stirred tank	stirred tank	Couette-Taylor
\tilde{d}_p (μm)	140-980	230, 330	70-500
$\tilde{\rho}_p/\tilde{\rho}_c$	1.15-8.41	1.15, 2.45	≈ 2.5
I_r	$\gtrsim 0.3$	$\gtrsim 0.6$	$\lesssim 0.5$
Observed Behavior	settling reduced $\tilde{d}_p/\tilde{\eta}_K > 10$	settling reduced $\tilde{d}_p/\tilde{\eta}_K > 5$	$500 \mu\text{m } C_D \approx 40 \times C_{D_o}$ $70 \mu\text{m } C_D \approx C_{D_o}$
minimum u_s/u_t when	0.4 $\tilde{d}_p/\tilde{\eta}_K \approx 20$	0.5 $\tilde{d}_p/\tilde{\eta}_K \approx 25$	0.2 $d_p/\eta_K \approx 30$
Proposed Mechanism	interaction with field	interaction with field	$\frac{C_D - C_{D_o}}{C_{D_o}} = 8.76 \times 10^{-4} \left(\frac{\tilde{d}_p}{\tilde{\eta}_K} \right)^3$

Table 7: Experimentally observed behavior for heavy particles versus $\tilde{d}_p/\tilde{\eta}_K$ or $\tilde{\eta}_K/\tilde{d}_p$. \tilde{d}_p is particle diameter, $\tilde{\rho}_p$ is particle density, $\tilde{\rho}_c$ is carrier fluid density, I_r is relative turbulence intensity, u_s is stirred tank settling velocity, u_t is unstirred tank settling velocity and $\tilde{\eta}_K$ is Kolmogorov microscale. (Note: I_r estimated from $\tilde{\eta}_K$.)

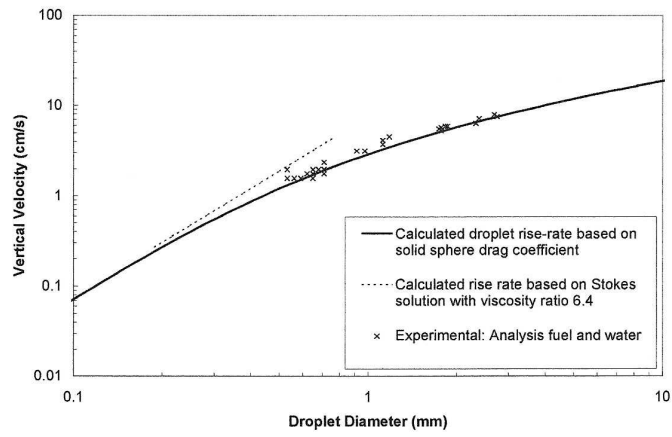


Figure 1: Friedman and Katz (Ref. 1) experimentally determined quiescent rise velocity for slightly buoyant oil droplets. “Analysis fuel” refers to slightly buoyant fuel oil. Used with permission.

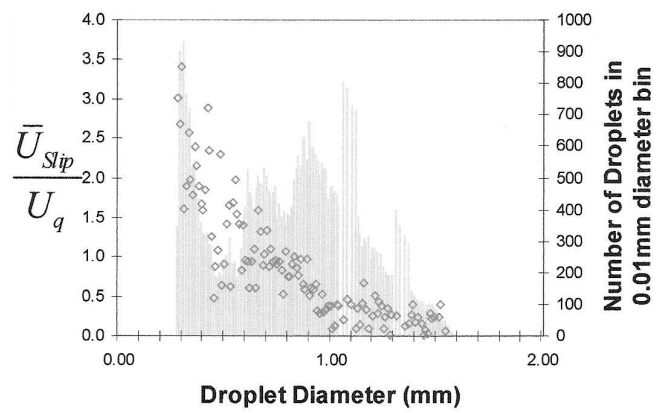


Figure 2: Friedman and Katz (Ref. 1) large facility L3 experimentally determined turbulent rise velocity, normalized by quiescent rise velocity, for slightly buoyant oil droplets in isotropic turbulence. Histogram reference to right scale shows number of droplets in analysis bin of 0.01 mm. Data points, \diamond , referenced to left scale show mean rise rate. Used with permission.

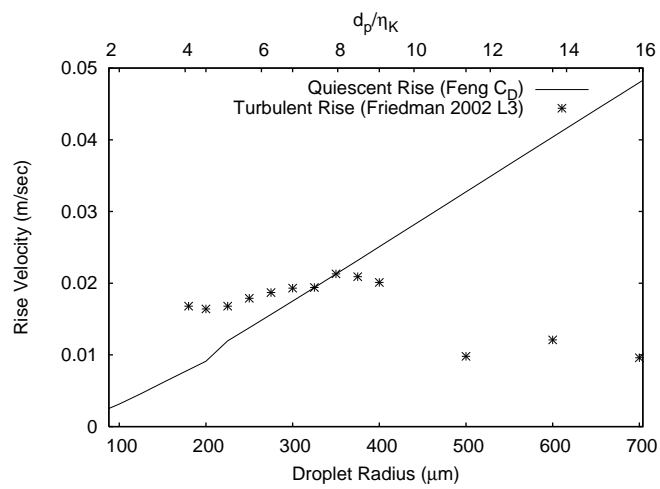


Figure 3: Friedman and Katz (Ref. 1) experimentally determined turbulence rise data for slightly buoyant oil droplets in large facility L3 compared with quiescent rise approximation using Feng and Michaelides (Ref. 9) C_D with viscosity ratio of 6.41. Upper horizontal scale shows droplet diameter normalized by Kolmogorov microscale, d_p/η_K .

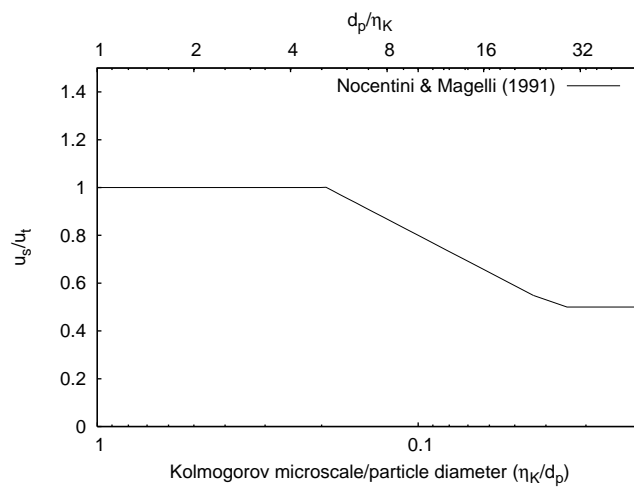


Figure 4: Stirred tank settling velocity normalized by unstirred tank settling velocity, u_s/u_t , versus Kolmogorov microscale normalized by particle diameter, η_K/d_p (Nocentini and Magelli Ref. 10). Upper horizontal scale shows particle diameter normalized by Kolmogorov microscale, d_p/η_K .

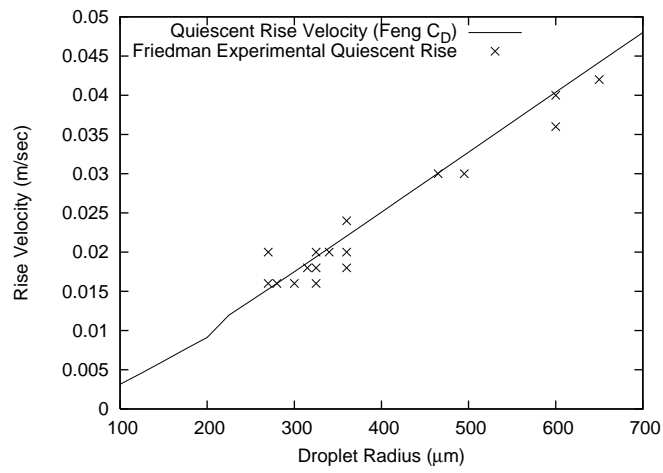


Figure 5: Friedman and Katz (Ref. 1) experimentally determined quiescent rise data for slightly buoyant oil droplets compared with numerical approximation using Feng and Michaelides (Ref. 9) C_D .

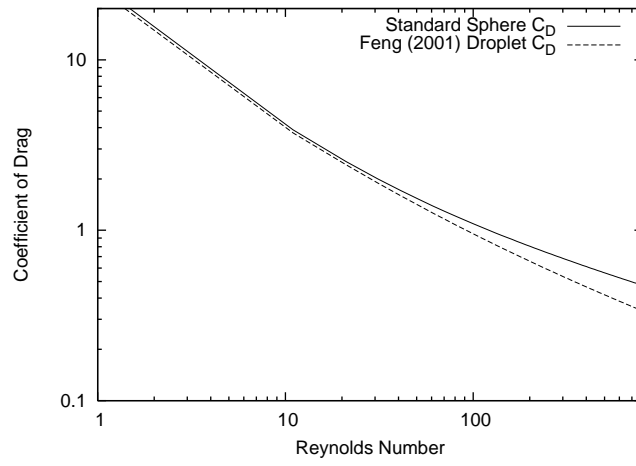


Figure 6: Standard sphere C_D and Feng and Michaelides (Ref. 9) C_D for fuel oil in water versus Reynolds number.

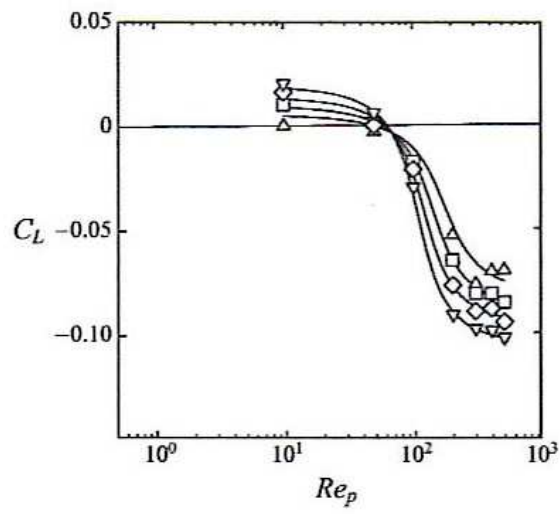


Figure 7: Kurose and Komori (adapted from Ref. 23) lift coefficient C_L for a stationary sphere in linear shear flow: \triangle , $\alpha^* = 0.1$; \square , $\alpha^* = 0.2$; \diamond , $\alpha^* = 0.3$; ∇ , $\alpha^* = 0.4$. α^* is dimensionless shear.

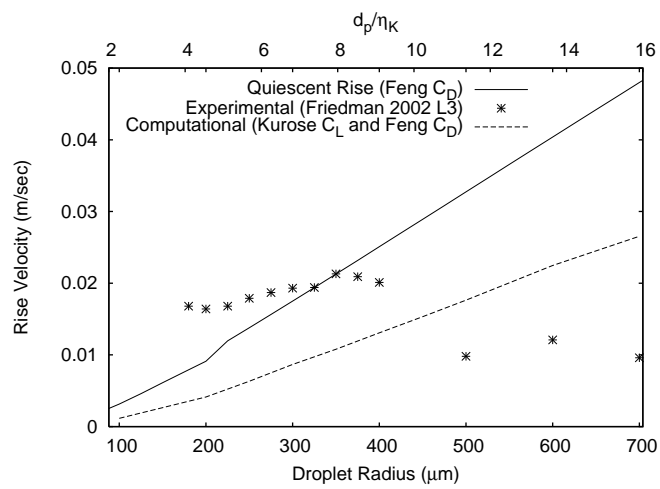


Figure 8: Friedman and Katz (Ref. 1) experimentally determined turbulence rise data for slightly buoyant oil droplets compared with baseline numerical approximation using Feng and Michaelides (Ref. 9) C_D and Kurose and Komori (Ref. 23) C_L . Upper horizontal scale shows droplet diameter normalized by Kolmogorov microscale, d_p/η_K .

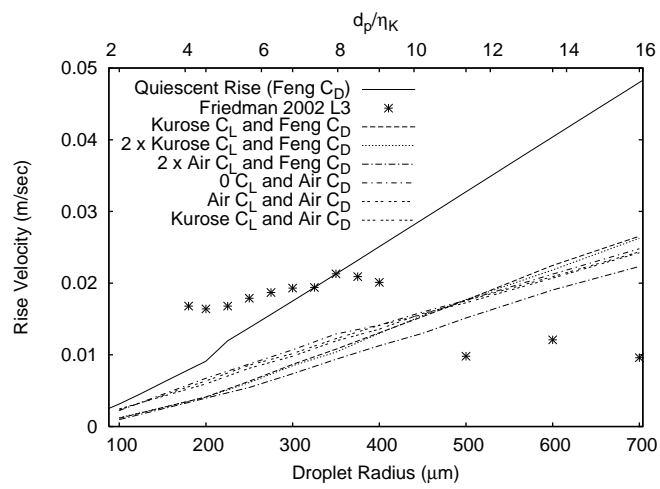


Figure 9: Simulation results for various combinations of lift and drag coefficients compared with experimental turbulent rise results of Friedman and Katz (Ref. 1). Upper horizontal scale shows droplet diameter normalized by Kolmogorov microscale, d_p/η_K .

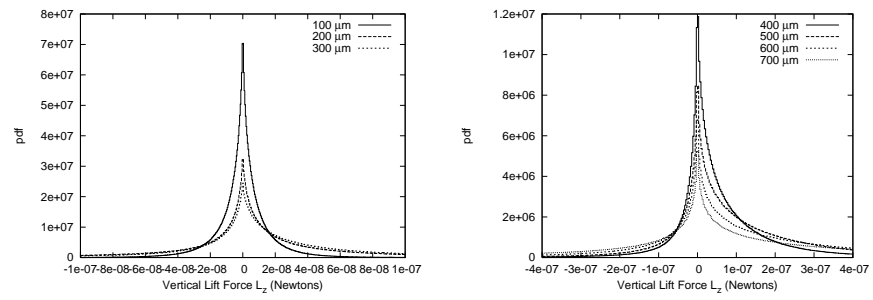


Figure 10: Probability density functions of the droplet lift force in the vertical direction, L_z , versus droplet radius.

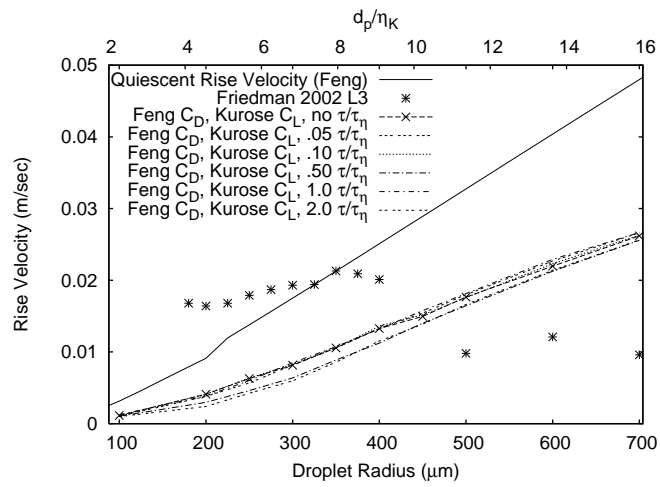


Figure 11: Simulation results for Basset force with time history of $\tau/\tau_\eta=0.05, 0.1, 0.5, 1.0,$ and 2.0 compared with experimental turbulent rise results of Friedman and Katz (Ref. 1). τ_η is Kolmogorov time scale. All simulations used Feng and Michaelides (Ref. 9) C_D , Kurose and Komori (Ref. 23) C_L and $C_{VM} = 1/2$. Upper horizontal scale shows droplet diameter normalized by Kolmogorov microscale, d_p/η_K .

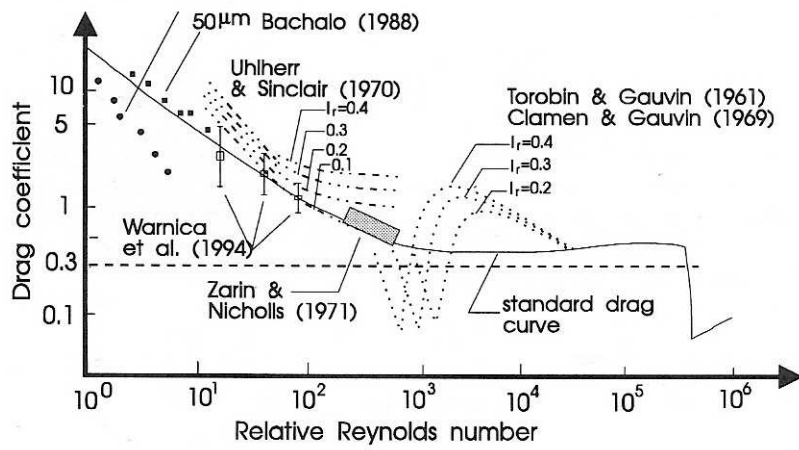


Figure 12: Standard drag curve and selected experimental drag curves for relative turbulence intensity $I_r > 0$ (adapted from Crowe *et al.* Ref. 19).

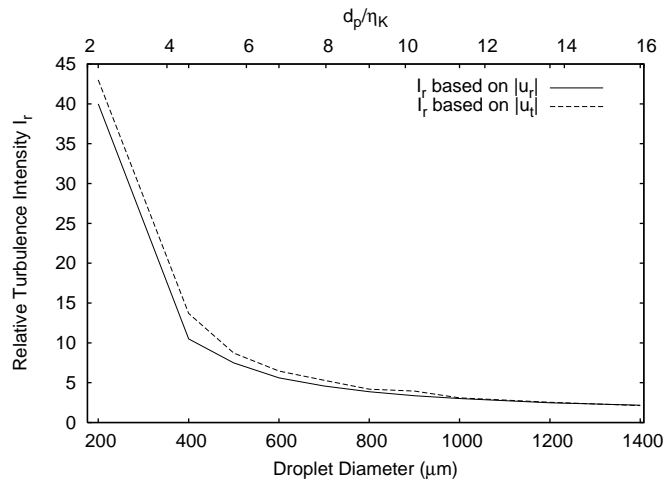


Figure 13: I_r based on relative and terminal droplet velocity versus oil droplet diameter for simulation of Friedman and Katz (Ref. 1) large facility L3 with $\tilde{\eta} \approx 88 \mu m$. Upper horizontal scale shows droplet diameter normalized by Kolmogorov microscale, d_p/η_K .

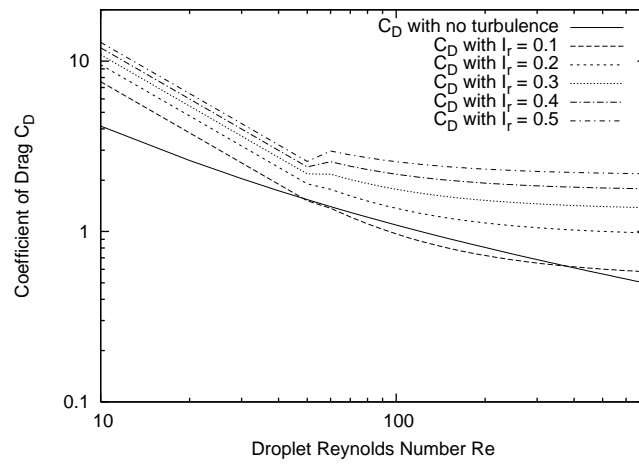


Figure 14: Variation in C_D versus Re_p and I_r following Uhlherr and Sinclair (Ref. 44).

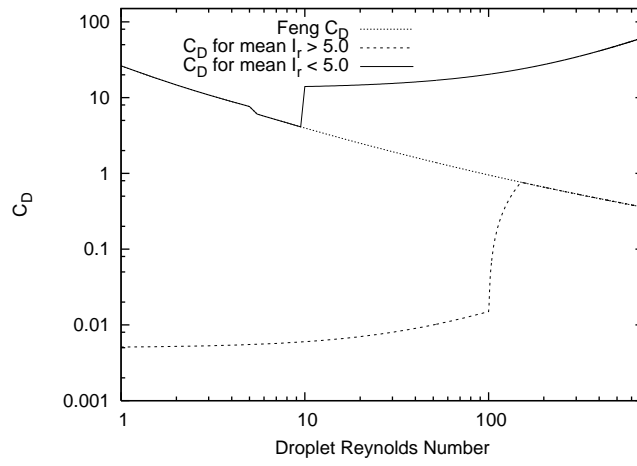


Figure 15: Modified C_D correlations used versus Re_d and mean turbulence intensity \bar{I}_r .

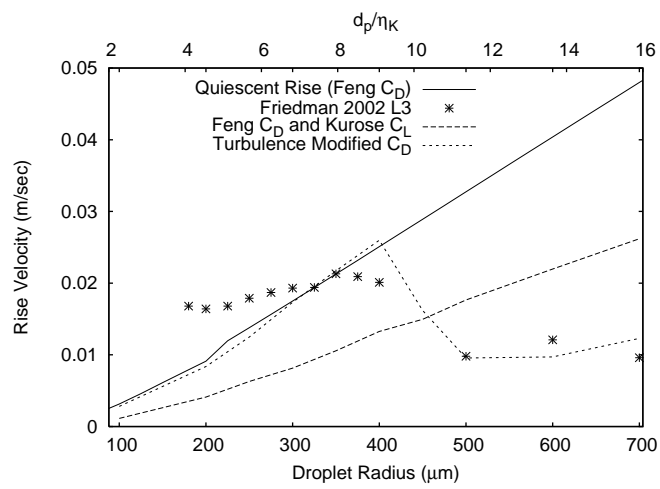


Figure 16: Simulation results for variation in C_D due to mean turbulence intensity \overline{I}_r compared with experimental turbulent rise results of Friedman and Katz (Ref. 1). Upper horizontal scale shows droplet diameter normalized by Kolmogorov microscale, d_p/η_K .

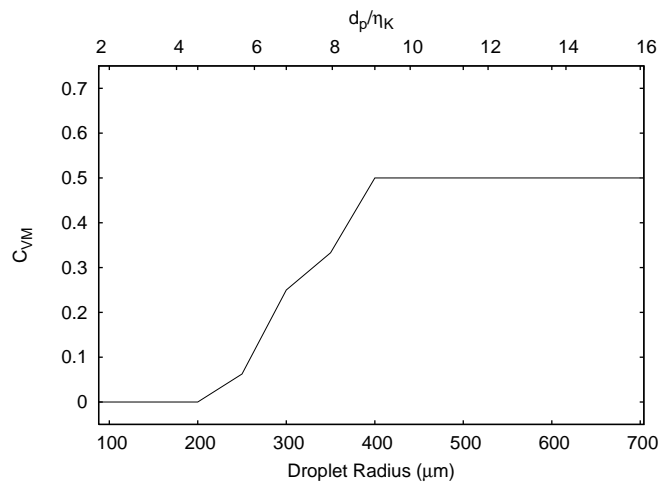


Figure 17: Modified C_{VM} used versus droplet radius. Upper horizontal scale shows droplet diameter normalized by Kolmogorov microscale, d_p/η_K .

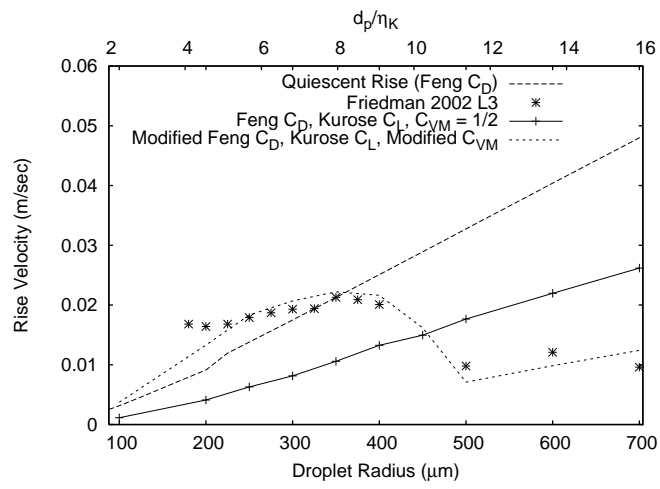


Figure 18: Simulation results for variation in C_D and C_{VM} due to mean turbulence intensity \bar{I}_r compared with experimental turbulent rise results of Friedman and Katz (Ref. 1). Modified C_{VM} is that shown in Figure 17. Upper horizontal scale shows droplet diameter normalized by Kolmogorov microscale, d_p/η_K .